LISE++

version 6.2

Contents:

1. Transport envelope calculation package

The envelope calculation package permits to visualize the dynamics of changes in distributions along the spectrometer. Use the menu "Plot->Envelope Plot" or the icon [icon] in the toolbar to load the new utility. The code builds envelope plots for horizontal and vertical angular distributions, horizontal and vertical spatial distributions, and energy and momentum distributions (see Fig.1). The code extracts the mean value of the distribution (red line in Fig.1) at the beginning and at the end of each block. Green and blue lines show left and right positions corresponding to the half-maximum amplitudes of these distributions.
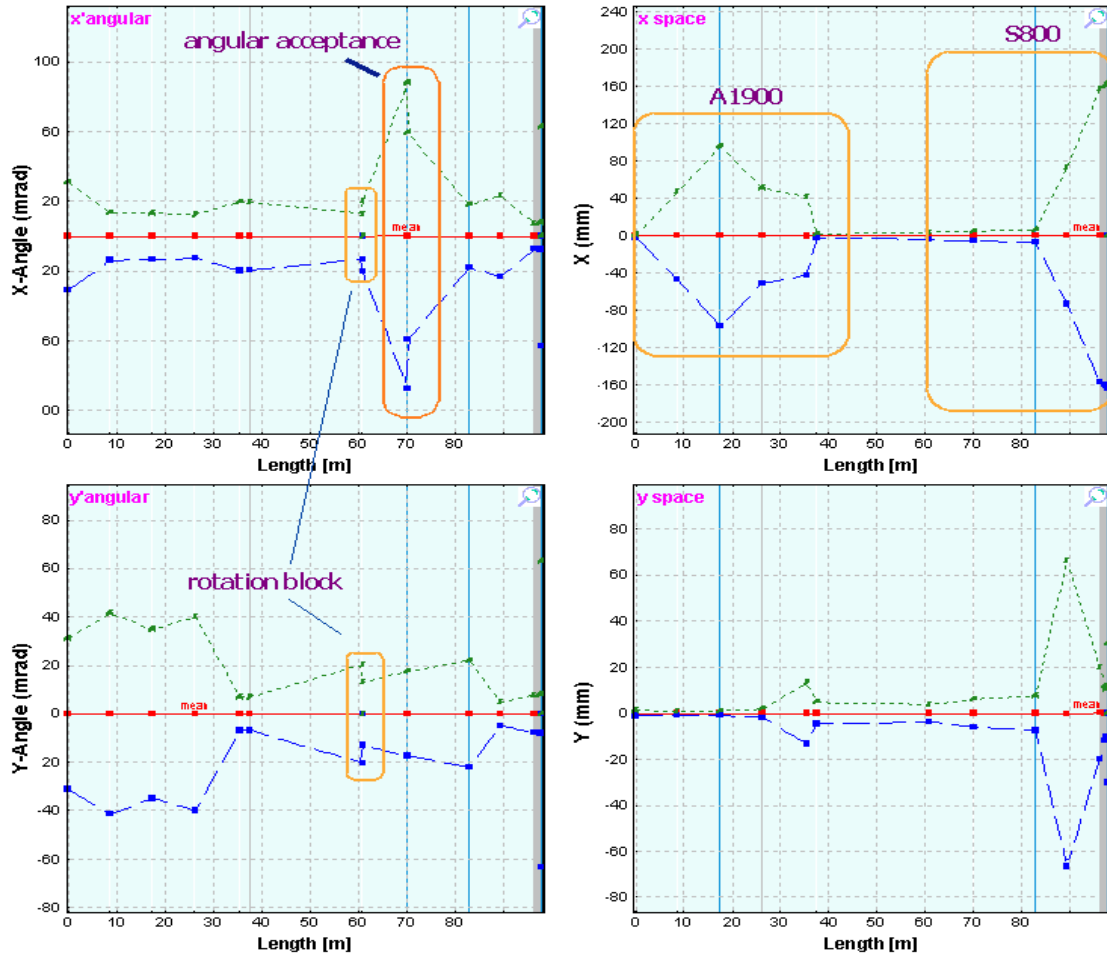
Fig.1. ^{32}S envelope for the configuration A1900_S800_d0. The spectrometer is set to the fragment ^{32}S. The round rectangle "angular acceptance" shows the cut of horizontal angular distribution by the acceptance of the second part of s800 beam-line spectrometer.

Fig.2. ^{32}S horizontal spatial distribution envelope for the configuration described in Fig.1, but the spectrometer set to a 3% higher magnetic rigidity.
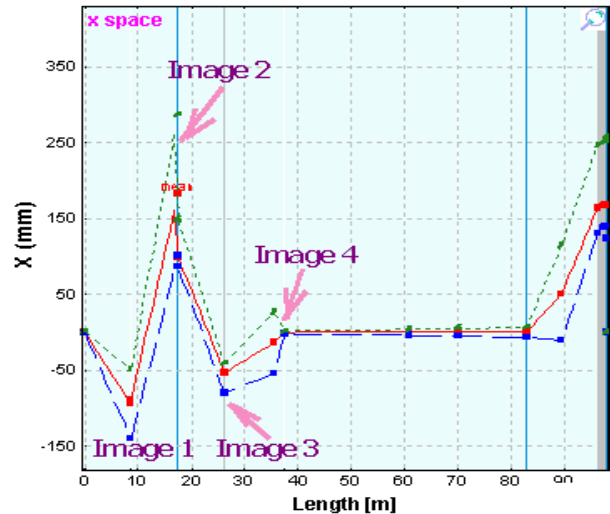
Fig.2 shows for comparison the ^{32}S horizontal spatial distribution for the spectrometer tuned to magnetic rigidity 3% above the ^{32}S optimal value (Fig.1).

The envelope package allows to debug the code calculations, to see the evolution of the distributions and their changes due to energy loss in materials (wedge) and the influence of slits.

Use "zoom" plot to see evolution momentum or energy distributions between detectors.

2. Code "Charge"

"CHARGE" is a user program developed at GSI which calculates atomic charge-changing cross sections, charge-state evolutions, and equilibrium-charge-state distributions for bare, H-, and He-like relativistic heavy ions penetrating through matter. The code "Charge" [Sch98] has been translated into C++ and is now part of the "LISE++" package. The source code (FORTRAN) was kindly provided by colleagues from GSI. The "Charge" code can be loaded by using the icon ⊙ in the toolbar or the menu "Utilities". The program interface window is shown in Fig.4. "Equilibrium thickness
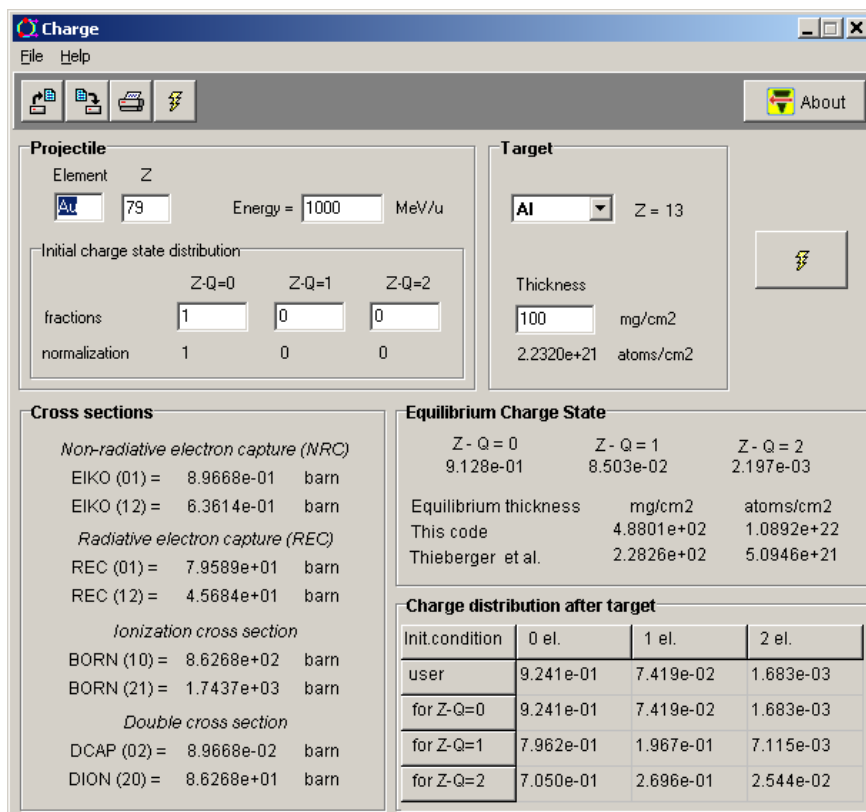
Fig.4. *The "Charge" code (version for MS Windows) is in action*
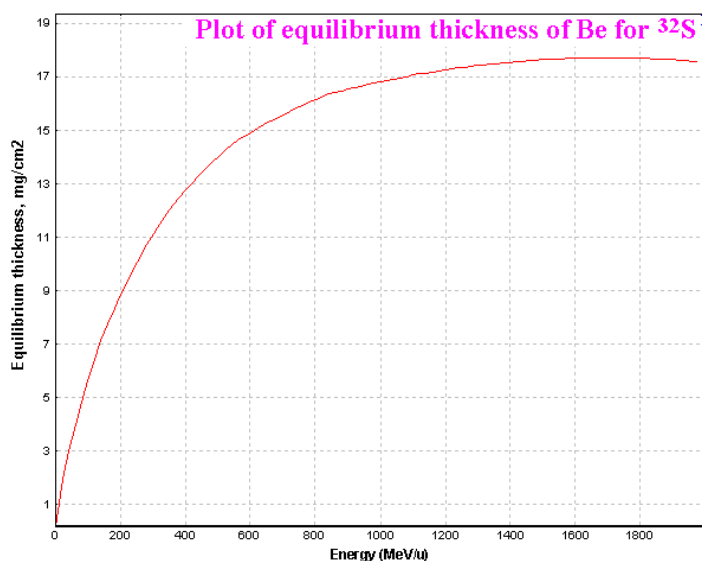
Fig.3. *Equilibrium thickness for ^{32}S in material Be.*

versus projectile energy" plot (Fig.3) can be loaded in LISE++ (menu "Utilities"). LISE++ uses Thierberger's [Thi85] definition of the equilibrium thickness from the code "Charge".

It is possible also to see the equilibrium thickness value in the "Physical calculator".

The program "Global" [Sch98] will be soon adapted for "Windows" and will be used in LISE++ for calculations of charge states distributions.

3. Brho (Erho) analyzer dialog

The Brho / Erho analyzer dialog is developed to calculate and plot a trajectory of ions in the magnetic / electrical dipoles depending on energy and emittance of beam and settings of the dipole. The utility can help to calculate a position for a primary beam trap in the chamber dipole to avoid scattering of a primary beam on walls of the dipole chamber. The dialog is loaded from the menu "Utilities → Brho Analyzer". The Brho (Erho) analyzer supports magnetic and electric dipoles. The dialog in the "magnetic dipole" mode is shown in Fig.5. The switching between modes is made by choice of a field of dipole. The "magnetic dipole" mode is chosen in case of input of $B\rho$ or B values, in the case of $E\rho$ or E values, accordingly the "electrostatic dipole" mode will be applied. The user can see the mode used in the window "A" of the dialog (see Fig.5). An example of the "electrostatic dipole" mode is presented in the chapter "4.2. Electrostatic dipole".
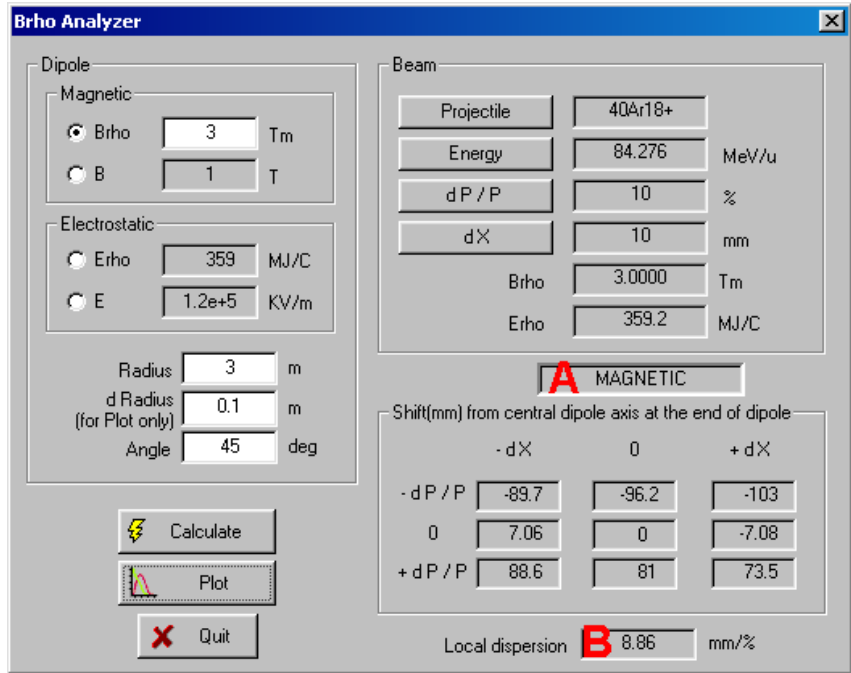

Fig.5. *Brho(Erho) analyzer dialog in action of "magnetic" mode.*

It is always assumed, that the incoming beam is parallel to an optical axis of spectrometer. The Brho analyzer calculates a local dispersion in the end of the dipole by using relations:

$$D = \frac{X_{+dP/P} - X_{-dP/P}}{2 \cdot dP/P} [mm/\%] \qquad dP/P \neq 0 \text{ and } (X_{+dP/P} \cdot X_{-dP/P}) < 0 \qquad /1/$$

$$D = \frac{X_{P_{beam}}}{P_{beam}/P_0 - 1} \cdot 100 \, [mm/\%] \qquad dP/P \to 0 \text{ or } (X_{+dP/P} \cdot X_{-dP/P}) > 0, \qquad /2/$$

where P_{beam} is the user's adjusted momentum of the beam projectile, P_0 is the momentum of projectile corresponding to the dipole central line. Local dispersion is given in the field marked by "B" (see Fig.5).

The program calculates 9 trajectories proceeding from combinations of 2 sets with three parameters characterizing beam (-dX, 0, +dX) and (-dP/P, 0, +dP/P). Numerical values in the exit of the dipole can be visualized in the dialog window. The sequence of steps is given next:

- Determine beam characteristics (mass, charge, energy and emittance (dP/P and dX),
- Choose magnet entry field and enter the value,
- Enter the dipole parameters: radius, half-width of dipole chamber (d_radius), and angle (d_radius is used only to show a chamber boundaries on the plot),
- Press the "Calculate" button to calculate trajectories, and then "Plot" to draw calculated trajectories.

As an example trajectories calculated for four different initial conditions are shown in Fig.6.
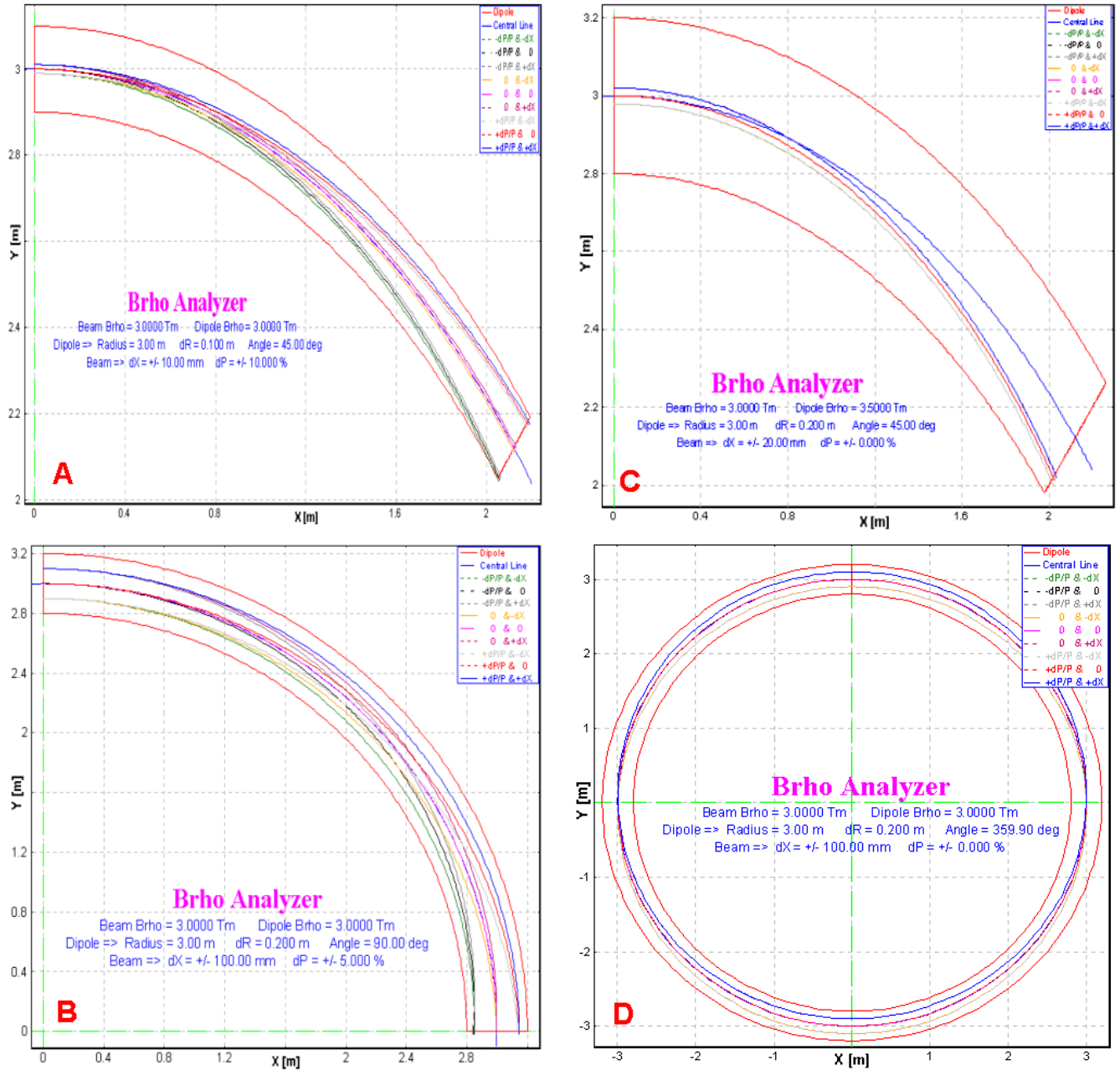
Fig.6. *Brho analyzer plots for four different initial conditions. Initial conditions are listed in Table 1.*

Table 1. *Initial parameters of the primary beam and dipole settings for Fig.6.*

Plot	Beam Brho, *Tm*	Dipole Brho, *Tm*	R *m*	DR *m*	Angle *degree*	dX ± *mm*	dP ± %
A	3.0	3.0	3	0.1	45	**10**	**10**
B	3.0	3.0	3	0.2	90	**100**	**5**
C	3.0	**3.5**	3	0.2	45	**20**	0
D	3.0	3.0	3	0.2	360	**100**	0

4. New optical blocks

Three new optic blocks based on magnetic dipoles have been developed:

- Compensating dipole
- Electric dipole
- Gas-filled magnetic dipole.

Electric dipole and gas-filled magnetic dipole blocks (as well as configuration files created on their base) are still under construction and will be more developed and optimized very soon in the experimental groups in operating conditions.

All three new blocks are intended for low-energy beam applications. In this context the further development of reaction models (fusion-evaporation, fission) is planned, and also use of charge state models at significantly lower energies. Please note, that the user can enter a production cross-section manually, instead of use "LisFus" model calculations. For this purpose it is necessary to set the option "File" in the dialog "Options⇒Preferences" and enter a cross section value in the dialog "Cross sections" (menu "Options"). The red square in the right bottom corner of an isotope cell in the table of nuclides indicates that a cross section value from a file is used.
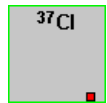
4.1. Compensating dipole

Compensating dipole block has already been realized in the code LISE as the block "D6" (http://groups.nscl.msu.edu/lise/3_4/lise_3_4.html). This block represents a magnet on a platform that it is possible to incline, so that the global dispersion after the block will be equal to zero. In the LISE++ code the compensating dipole may be used now after dispersive block (not only after the Wien velocity filter as it was done in the code LISE) to compensate global dispersion. The compensating dipole block can be used for the spectrometer MARS

Fig.7. Compensating dipole in the "Set-up" window.

(TAMU), and for LISE3 and VAMOS at GANIL. Compensating dipole characteristics in the "Set-up" window is shown in Fig.7, where **Br** is the magnetic rigidity (Brho) [Tm], **A** is the inclination angle of the magnet [deg], **DG** is the global dispersion behind this block [mm/%].
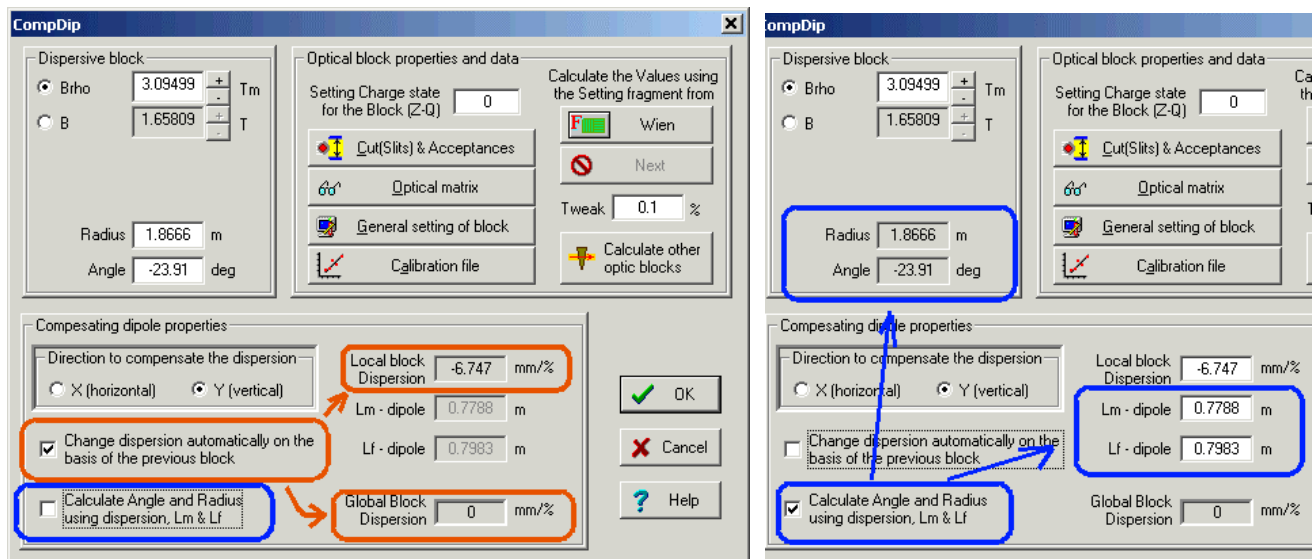
Fig.8. *The compensating dipole dialog. Left and right picture show different modes of compensating dipole settings.*

Some new features have been added. It is now also possible to input the local dispersion manually as well as the radius and the angle of the dipole (see Fig.8). The configuration file "LISE3.lcn" for the LISE spectrometer with Wien velocity filter and the compensating dipole D6 is included in the standard LISE++ package. An example of a simulation using the LISE3 configuration is shown in Fig.9.
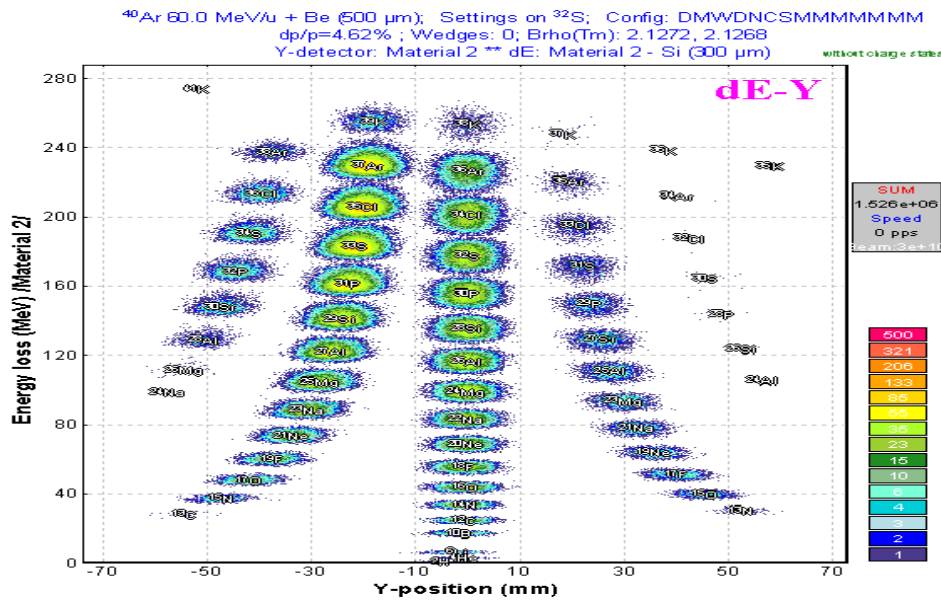

Fig.9. Plot of energy loss versus vertical position in final focal plane for the LISE3 configuration file. The vertical plane represents a selection with A/Q dispersion.

4.1.1. MARS spectrometer configuration

A preliminary configuration (file "TAMU-MARS.lcn") for the MARS spectrometer [Tri89] has been developed. The scheme of the spectrometer is shown in Fig.10. An example to produce the secondary beam of ions ^{8}He with the MARS spectrometer is provided in the file "TAMU-Mars_8He.lpp". The two-dimensional particle identification plot and the selection plot to produce ^{8}He secondary beam are show in Fig.11 and 12. It is planned to optimize the MARS configuration in future experiments.
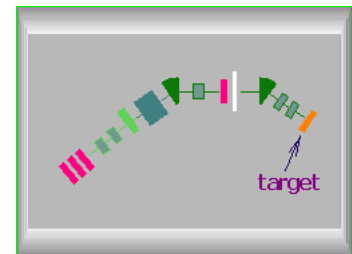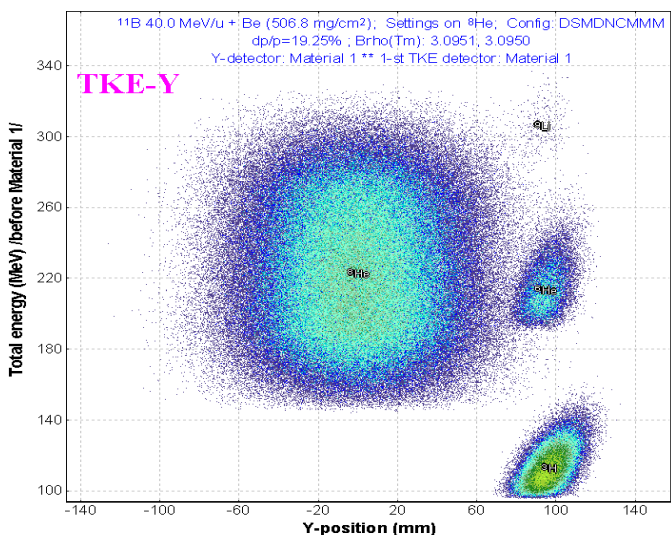

Fig.10. MARS spectrometer scheme

Fig.11. The plot of total kinetic energy versus vertical position in the final focal plane of the MARS spectrometer set to produce the secondary beam of ^{8}He.
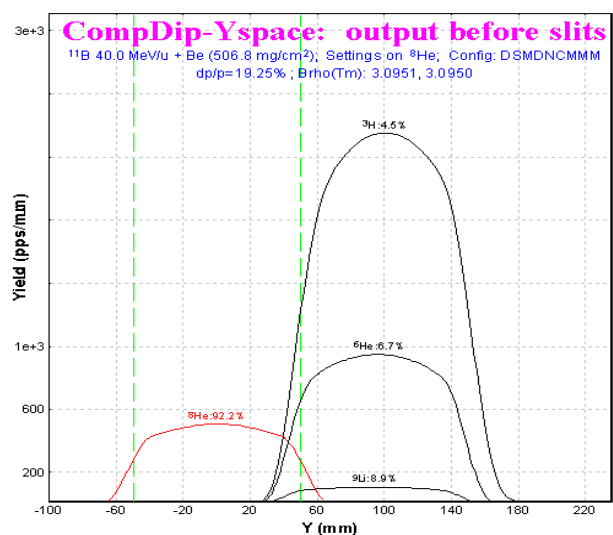
Fig.12. Vertical selection plot after the compensating dipole.

4.2. Electrostatic dipole

The new physical value "electric rigidity" ("Erho") has been added to physical values family of the code. Electric rigidity represents multiplication of electric field and dipole radius, and is characterized the settings of electrostatic dipole in analogy to the magnetic dipole and magnetic rigidity. Electric rigidity can be calculated as other physical values (Energy of projectile, Range, Brho etc) by means of the "Physical calculator" dialog.

The code assumes that electric field in the electrostatic dipole is always uniform and is equal to U/d, where U is the voltage, and d is the gap between plates. Electric dipole window in the "Set-up" window is shown in Fig.13, where E is the electric field [KV/m], U is the voltage [KV], Er

Fig.13. *Electrostatic dipole window in the "Set-up".*

is the electric rigidity [MJ/C]. The Electrostatic dipole dialog is shown in Fig.14. The edit cell "Magnetic rigidity" in this dialog serves just to show the corresponding value for setting fragment (residual) and helps in the case of the combination of magnetic dipole and electrostatic dipole.
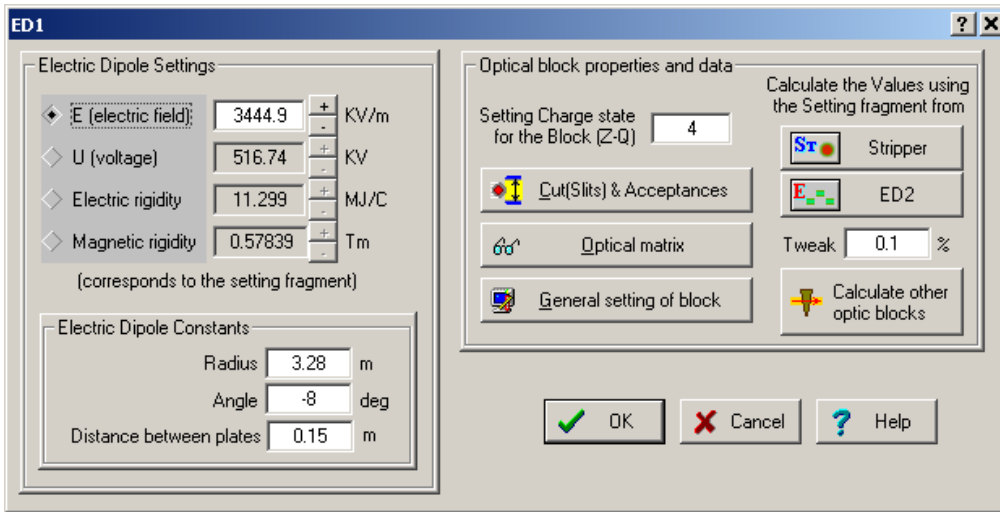
Fig.14. *The Electrostatic dipole dialog.*

Projectile trajectories in an electric dipole (as well as in a magnetic dipole) can be plotted in the dialog "Brho analyzer" (see chapter "3. Brho (Erho) analyzer dialog"). Similar to other optic dispersive blocks the electric dipole block uses the optical transport matrix with the dispersion determined by relation $x/(\Delta P/P)$. The code calculates the momentum of the ion (P_{dipole}) from the electric dipole settings. The spatial component x_P is calculated based on the dispersion, fragment momentum distribution, and P_{dipole}. The application of electric dipole mode in LISE++ is given in the following chapter on by example of the kinematic separator VASSILISSA.

4.2.1. The kinematic separator "VASSILISSA" configuration

The LISE++ configuration file (LISE/config/Dubna/vassilissa.lcn) of the kinematic separator VASSILISSA has been created using the article [Yer94] and TRANSPORT code file for this separator which was kindly provided by V.Schepunov. The scheme of the spectrometer is shown in Fig.15. As in [Yer94] the reaction ^{22}Ne(100MeV) + ^{197}Au(0.35 mg/cm^2) $\rightarrow$ ^{215}Ac + 4n was chosen to calculate the recoil
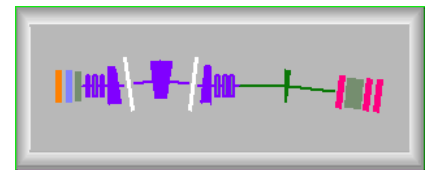
Fig.15. *The VASSILISSA separator scheme*

transmission for separator. The file "vassilissa_22ne_Au_charge_states.lpp" with these settings is included in LISE++ package and can be found in the directory "LISE\files".

4.2.2. Tuning the spectrometer for fusion-evaporation residue

Procedure to calculate the rate of fusion-evaporation products:

- Set "Fusion->Residual" as reaction in the dialog "Production mechanism";
- Select your spectrometer in the directory "LISE\Config" (or create new one);
- Enter the primary beam characteristics in the dialog "Projectile (Beam);
- Enter the target characteristics;
- Enter the stripper (after target) characteristics, if stripper thickness is not 0;
- Set the option "Charge states" ON in the dialog "Preferences";
- Check energy loss, charge states and other calculation methods used in the code. For lower energy (less 10 MeV/u) it is recommended to use the following methods:

Charge states calculation	Leon [1] or Shima [2]
Energy Loss calculation	Ziegler [1]
Energy straggling	Atima [1]
Angular straggling	Particle Data Group [2]

- Select the fragment (residue) of interest (don't enter charge states now);
- Click the button "Compound" in the setup window of the code to get the fusion-residue information window (see Fig.16) to see calculations of charge states, energies etc.
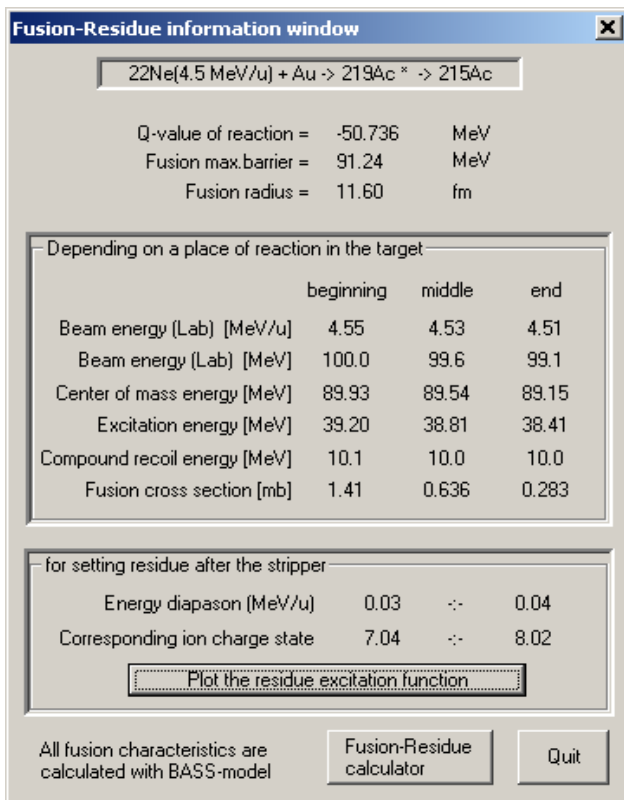

Fig.16. *The fusion-residue information window for the reaction $^{22}Ne(100MeV) + {}^{197}Au(0.35\ mg/cm^2) \rightarrow {}^{215}Ac + 4n.$*
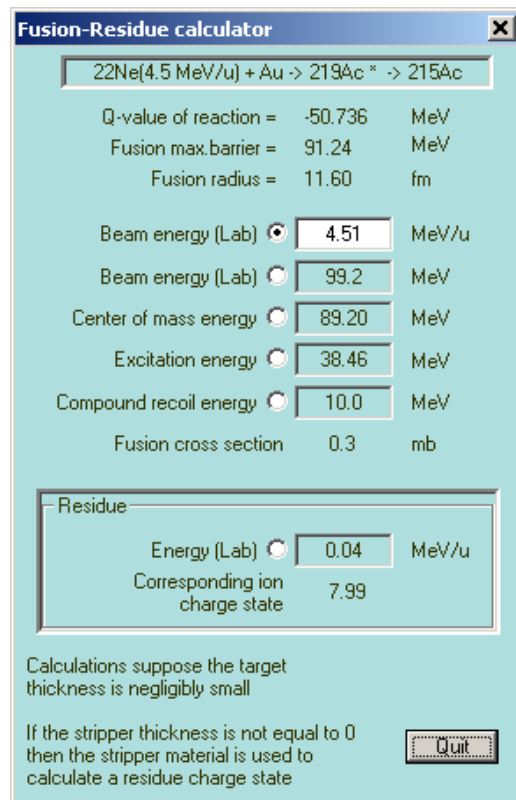

Fig.17. *The fusion-residue calculator can be loaded from the fusion-residue information window or from the menu "Calculations".*

- Depending on the corresponding charge state of the ion after the target (stripper) shown in the fusion-residue information window enter the charge state of the residual through the dialog "Setting fragment (residue)". Please keep in mind that it is also possible to estimate a charge state using the fusion-residue calculator (Fig.17);

- Calculate the spectrometer settings for the selected ion using the menu "Calculation" or the icon ⬇ in the toolbar;

- Calculate the selected ion transmission and rate by mouse right click over an isotope of interest or using the menu "Calculation→Transmission". If production cross section was not yet calculated or has not been entered manually, then the program will offer (see Fig.18) to calculate (A) the production cross section with the help of the LisFus model (without fission channel), or enter them manually (B). The user can enter 1. already known cross section, 2. calculate them using the PACE4 code 🎲, 3. enter any number, only to estimate a transmission.
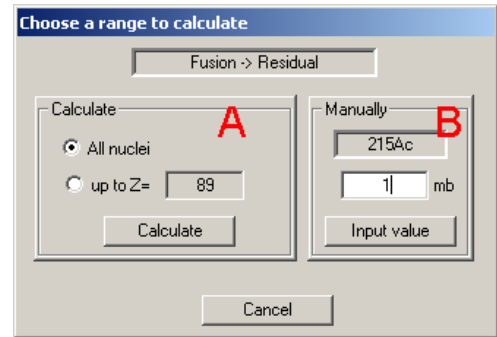

Fig.18.

4.2.3. Choice of charge state of ion to set the spectrometer

The mean ionic charge of ^{215}Ac after a carbon stripper is shown in Fig.19. It is possible to see that Winger's model (blue line) predicts a high value of ionic charge in the low energy region. Leon's (black line) and Schima's (green line) models are close to each other for low energies, however Shima's model underestimates a charge state with increasing energy. Therefore the model of Leon is recommended for calculations of charge states in the region between 0.5-5 MeV/u.

The comparison of various models of charge state calculations with experiments, and also energy regions of applications of models will be summarized in the next version documentation.
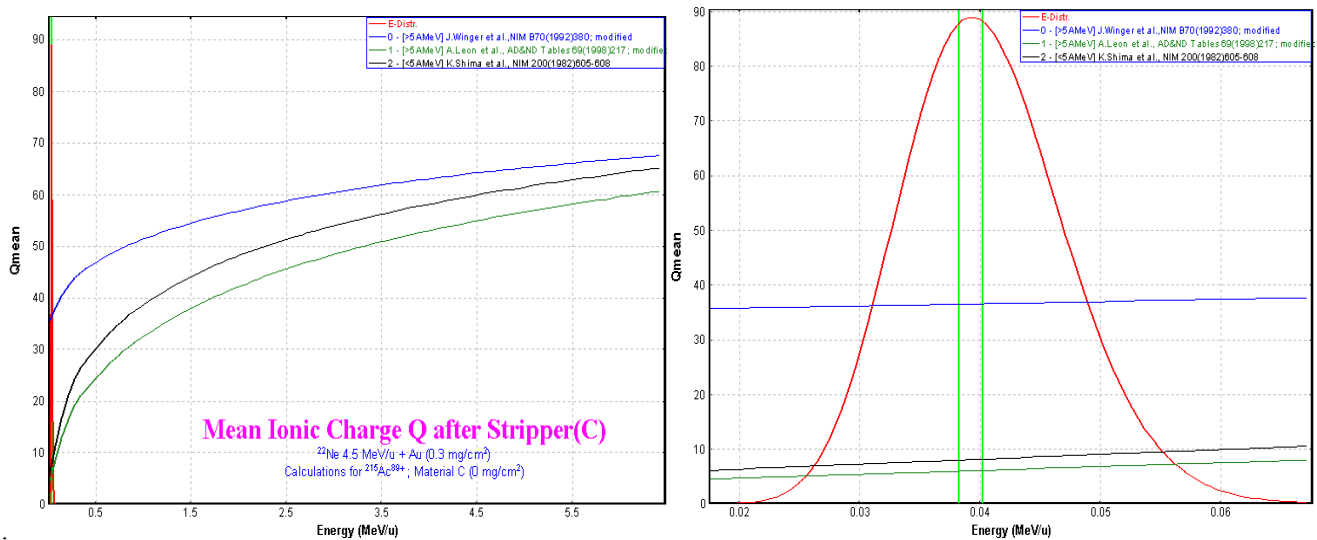

Fig.19. *Mean ionic charge of ^{215}Ac after a carbon stripper on the left plot shows in the energy diapason 0.0 – 6.0 MeV/u. The right plot is the same for the energy diapason 0.02÷0.07 MeV/u. The energy distribution of ^{215}Ac residue after the stripper is indicated by the red line. The energy distribution of different charge states of ^{215}Ac is shown in Fig.20.*
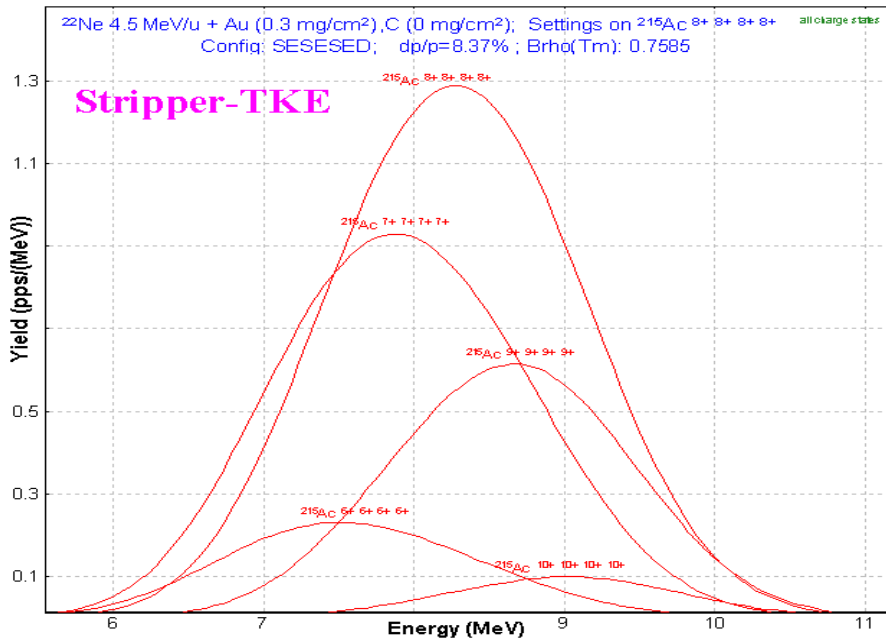
Fig.20. *Energy distribution of different charge states of ^{215}Ac residuals after a carbon stripper in the reaction $^{22}Ne(100MeV) + {}^{197}Au(0.35\ mg/cm^2) \rightarrow {}^{215}Ac + 4n$. The carbon foil ($0.35\ mg/cm^2$) is placed after the target to reset the charge distribution to equilibrium. $^{215}Ac^{8+}$ dominates the charge state distribution.*

4.2.4. Calculation of energy and angular distribution of fusion-evaporation residues

Fig.21 and Fig.22 compare evaporation residuals energy and angular distributions calculated by LISE++ and calculated using a Monte Carlo computer code [Yer94]. In the case of LISE++ all distributions have been calculated after a carbon stripper. The reactions used for the calculations are listed in Table 2. For LISE++ calculations the option "Charge state" was set off to sum all charge state distributions. LISE files for the examples discussed in the figure are located in LISE web-site:

> http://www.nscl.msu.edu/lise/6_2/examples/vassilissa_22ne_au.lpp
> http://www.nscl.msu.edu/lise/6_2/examples/vassilissa_31p_164er.lpp
> http://www.nscl.msu.edu/lise/6_2/examples/vassilissa_40ar_162dy.lpp

LISE++ uses $(d\sigma/d\Omega)_{x,y}$ "plane" (projection) angular distributions for transmission calculations. This means regular LISE's angular distributions (which the user can see in the plots) have been transformed to $(d\sigma/d\Omega)$ "space" distributions and then into distributions $(d\sigma/d\theta)$ to be compared with Monte Carlo calculations [Yer94]. In order to show a contribution of angular straggling calculations have been performed with and without angular straggling (see Fig.21 b & c). Angular straggling and the lateral range at low energies are discussed in the chapter "5.4. Angular straggling".

4.2.5. Suppression of the primary beam

Suppression of the primary beam is a more principal task in the region of nuclei with subnanobarn cross sections in heavy ions fusion-evaporation reactions. In this context it is necessary to take into account all possible factors capable to render influences on transmission/suppression of the primary beam. The current version of the code assumes energy and spatial broadening of the primary beam due to energy and angular straggling, but it does not take into account actual scattering of the beam in the target. In later versions of LISE++ it is planned to include a possibility to use a scattering primary beam. The initial emittance of the primary beam used to calculate transmission was set the following:

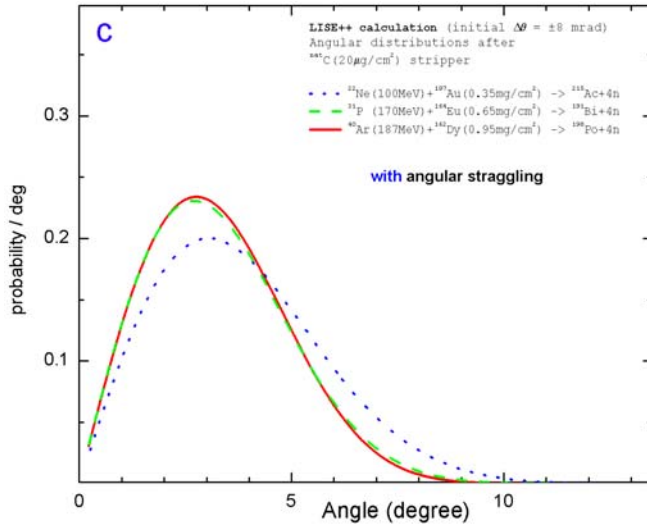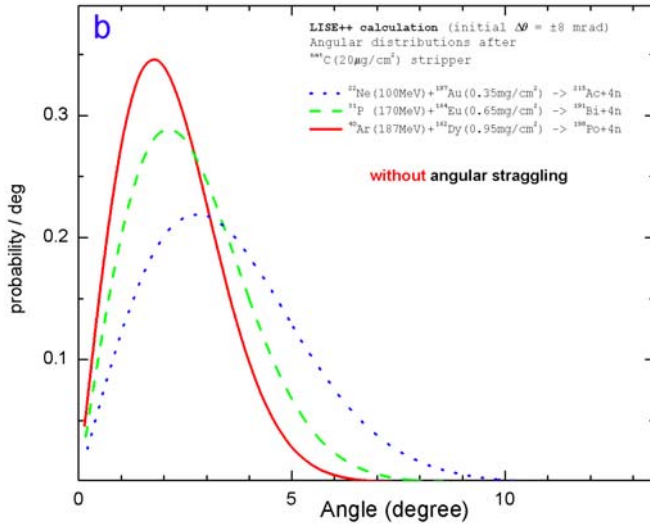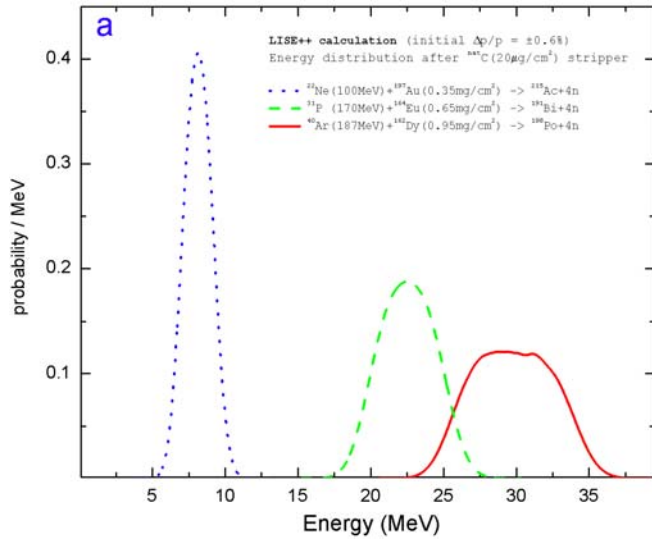$$x = y = \pm\ 2.5\ mm,\ x' = y' = \pm\ 8\ mrad,\ dP/P = \pm\ 0.6\ \%.$$

Fig.21. *LISE++ calculated energy (a), scattering angle without straggling contribution (b) and scattering angle with straggling contribution (c) distributions after the STRIPPER for evaporation residuals from the reactions listed in Table 2. See text for details.*
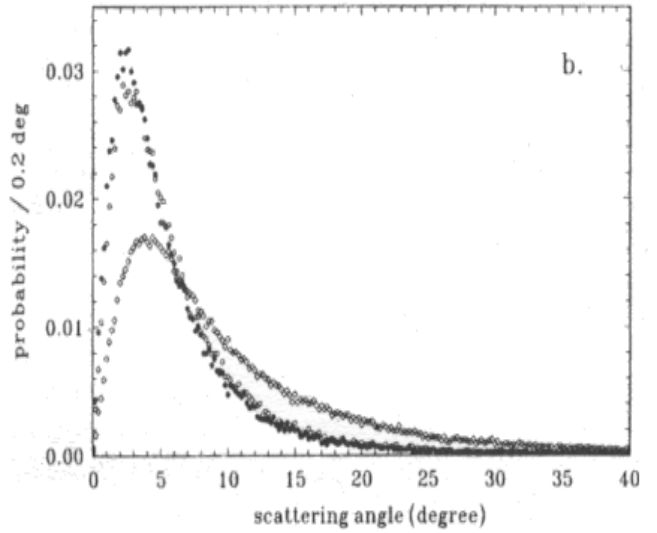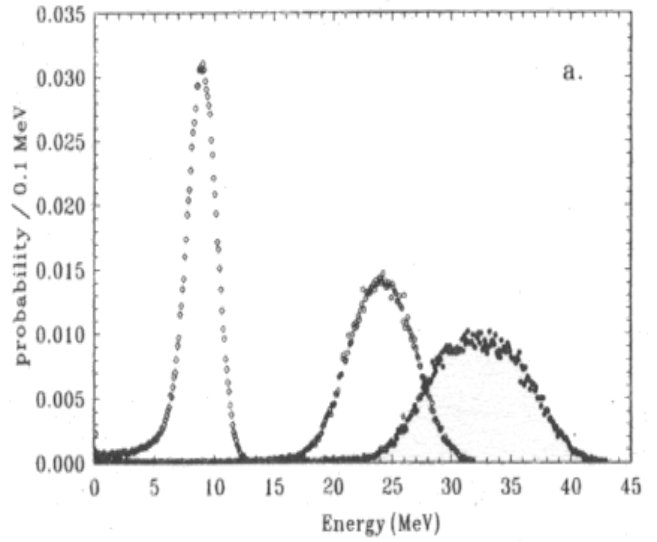

Fig.22. *Calculated energy (a) and angular (b) distributions [Yer94] for evaporation residuals from the reactions given in Table 2.*

Table 2. *Designations for Fig.21 and Fig.22*

for Fig.21	for Fig.22	reaction
•••	◊	^{22}Ne(100MeV) + ^{197}Au(0.35 mg/cm^2) → ^{215}Ac + 4n
– – –	O	^{31}P(170MeV) + ^{164}Er(0.65 mg/cm^2) → ^{191}Bi + 4n
—	●	^{40}Ar(187MeV) + ^{162}Dy(0.95 mg/cm^2) → ^{198}Po + 4n

The horizontal distributions of charge states of ^{215}Ac residual and primary beam particles from the reaction ^{22}Ne(100MeV) + ^{197}Au(0.35 mg/cm^2) after the first electric dipole of VASSILISSA separator are shown in Fig.23. The separator is set to the ion ^{215}Ac^{8+}. All blocks behind the first dipole in the separator configuration were set disable to get the primary beam horizontal distributions in Fig.23. The distributions were calculated assuming the dispersion being **position independent** from position in the horizontal plane.
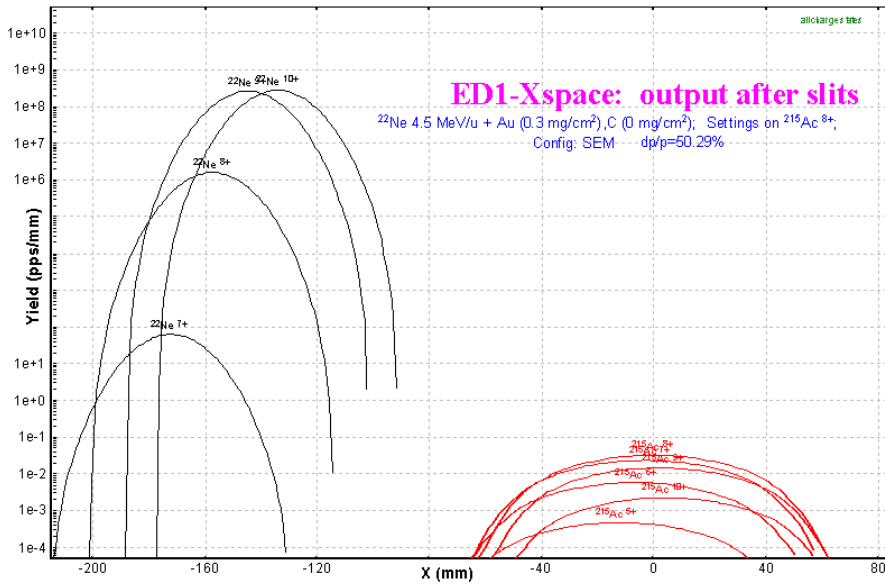
Fig.23. *Horizontal distributions of ^{215}Ac residuals (red) and primary beam charge states (black) after the first electric dipole. See a text for details.*
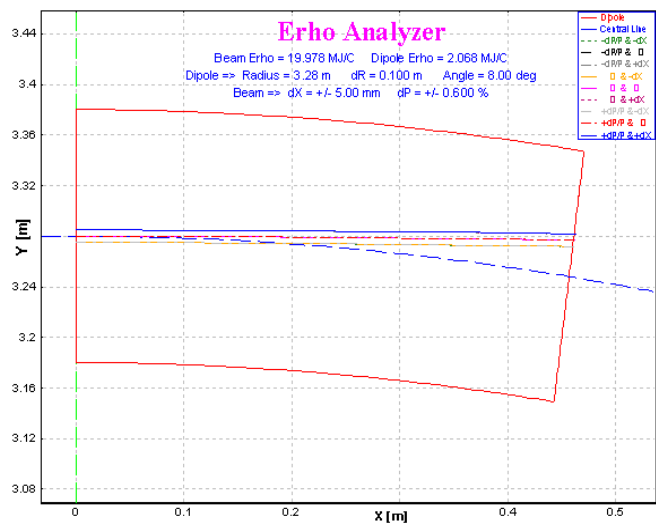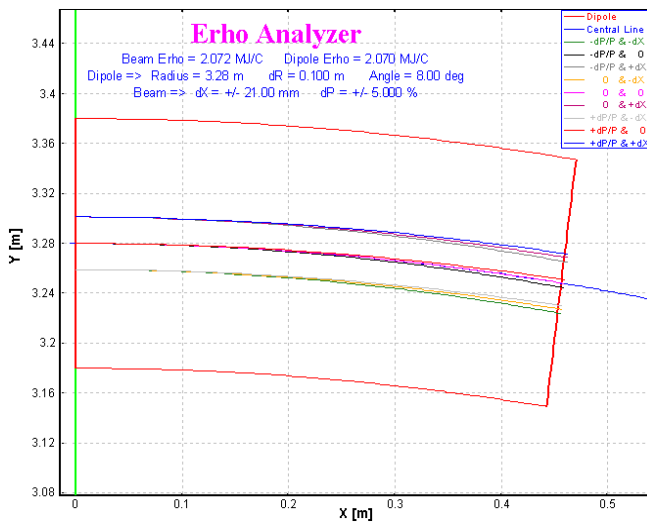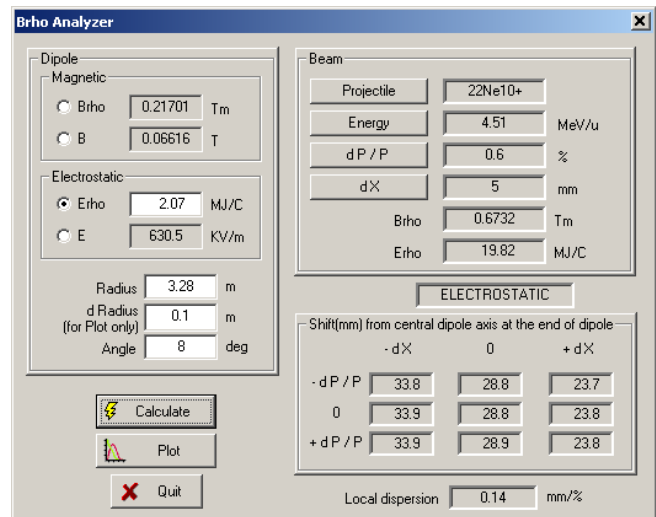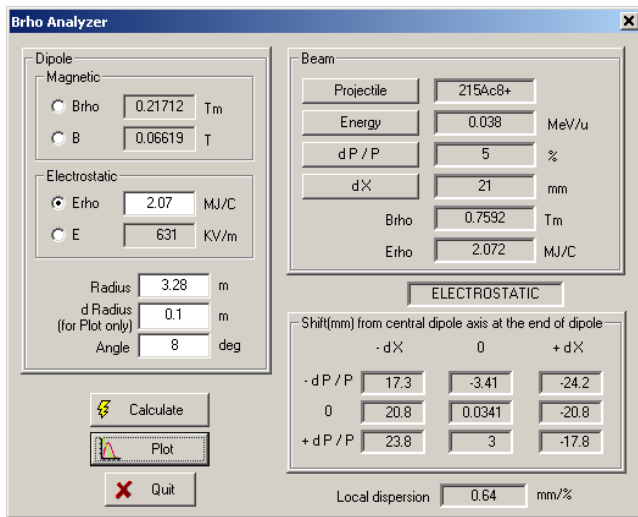

Fig.24. *Trajectory calculations for the residual ^{215}Ac^{8+} (left plots) and the primary beam charge state ^{22}Ne^{10+} (right plots) by the Brho(Erho) analyzer for the first dipole tuned to ^{215}Ac^{8+} in the reaction ^{22}Ne(100MeV) + ^{197}Au(0.35 mg/cm^2).*

It is easily seen from the picture that it is possible to separate residuals from the primary beam after the dipole. It is valid to consider a constant dispersion close to the central optical line for several percents of value dP/P. To show this statement and to determine a dispersion further away from a primary beam position in the dipole exit the calculations were made with the help of the Brho(Erho) analyzer. Initial conditions (energies, emittances) and calculated trajectories for the residual $^{215}Ac^{8+}$ and the primary beam charge state $^{22}Ne^{10+}$ are shown in Fig.24. It is obvious, that local dispersion in the case of ^{215}Ac is equal to 0.64 mm/% confirmed also by TRANSPORT (look the first dipole optical matrix in the configuration file), however in the case of primary beam the dispersion is equal to 0.14 mm/% and a shift of the primary beam from the optical axis results in 28 mm instead of 130 mm calculated by LISE++ assuming a constant dispersion. The residue $^{215}Ac^{8+}$ settings of the first dipole corresponds to an energy of 0.47 MeV/u for the primary beam charge state $^{22}Ne^{10+}$. The ratio of the primary beam momentum after the reaction and the momentum from dipole setting $P_{(22Ne)}/P_{dipole\ (22Ne10+)}$ is approximately equal to 3. Fig.25 shows calculated distributions of the horizontal position at the exit of the dipole from the ratio P/P_0 for electric and magnetic dipoles.
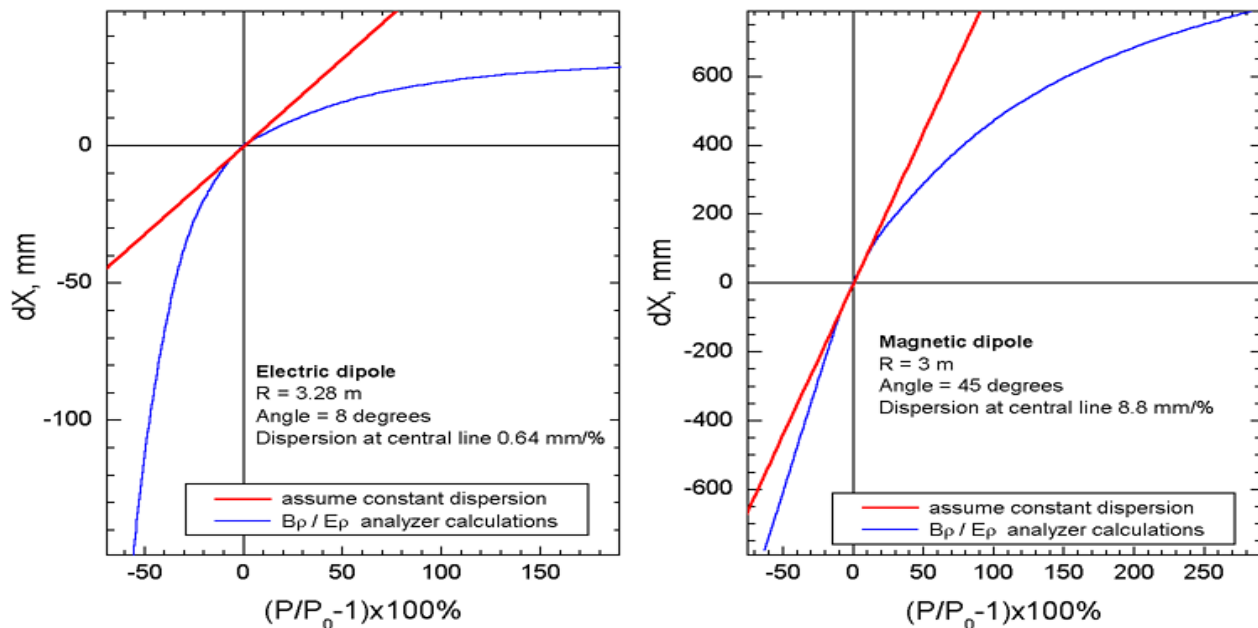
Fig.25. Horizontal position at the exit of dipole versus ratio (P/P0-1)·100% for electric (left) and magnetic (right) dipoles. Brho analyzer calculations are shown by blue color. Red lines show a shift from the central optical line assuming a constant dispersion.

In order to predict correctly the separation of residues and the primary beam it is planned to implement the following options:

- To add an opportunity to include a drift block after the dipole in the Brho(Erho) analyzer;

- To develop a subroutine to calculate a reduced dispersion for large values of dP/P;

- To insert a drift block between the two first dipoles in the configuration of the VASSILISSA separator to obtain a separation of residues from a primary beam.

4.2.6. Residue transmission calculation

An example of the transmission residues in the VASSILISSA separator from the reaction $^{22}Ne(100MeV) + ^{197}Au(0.35\ mg/cm^2)$ $\rightarrow\ ^{215}Ac^{8+}$ is given in the file "vassilissa_22ne_au_states.lpp" which is included in LISE++ package. The $^{215}Ac^{8+}$ envelope is shown in Fig.26.

The spectrum time-of-flight versus total energy at the VASSILISSA focal plane calculated by LISE++ is shown in Fig.27. The separator was optimized to get the maximum rate of $^{215}Ac^{8+}$ residues. Ne-like nuclei production cross sections were entered manually. Production cross sections of residues have been calculated within the LisFus model with the option quantum-mechanical transmission probability for the barrier. The curvature parameter $\hbar\omega$ was set to 3 MeV. Chapter "6. Sub-barrier fusion cross-section" provides more details on this option. Also this chapter presents results for residue production cross sections calculated within various reaction models and a comparison to experimental results. The separation efficiency, production cross section of residue ^{215}Ac, and rate of all charge states of residue ^{215}Ac as a functions of the target thickness are shown in Fig.28.

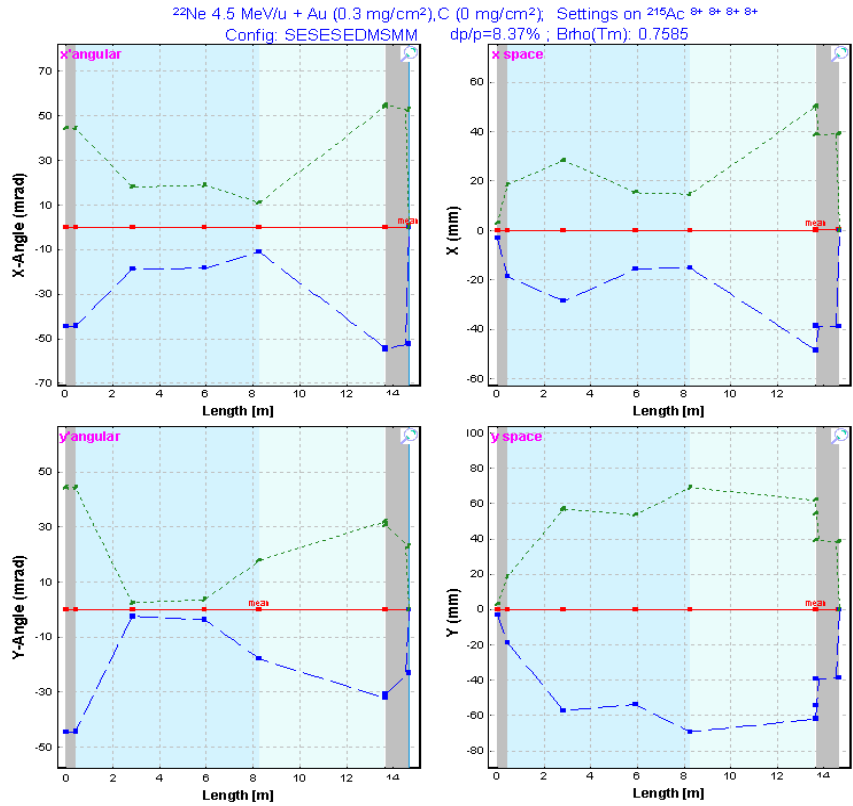**Fig.26.** $^{215}Ac^{8+}$ envelope in the reaction $^{22}Ne(100MeV) + ^{197}Au(0.35\ mg/cm^2)$ with the VASSILISSA separator. The separator was set to the ion $^{215}Ac^{8+}$.

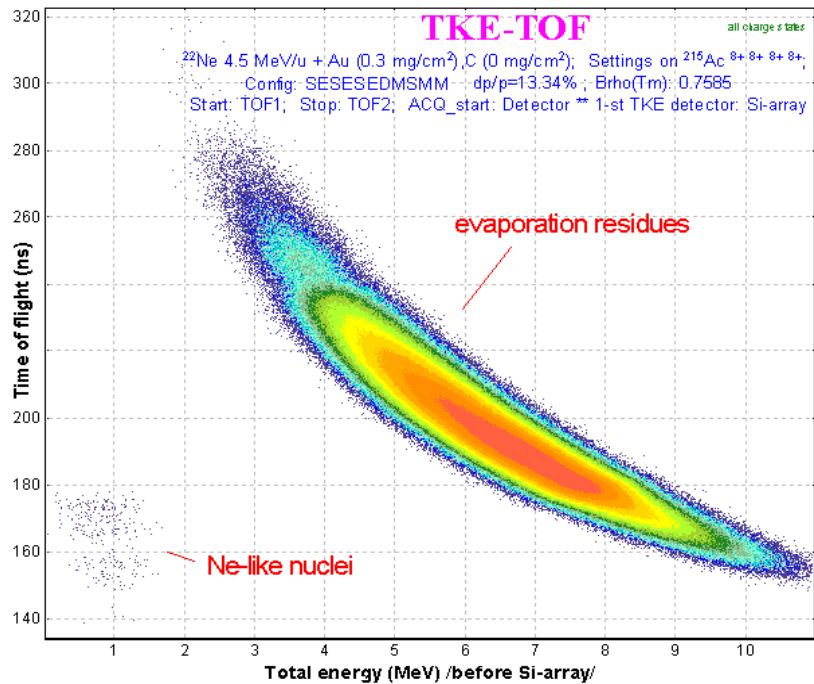**Fig.27.** Time-of-flight versus energy spectrum at the VASSILISSA focal plane calculated by LISE++ for the reaction $^{22}Ne(100MeV) + ^{197}Au(0.35\ mg/cm^2)$.
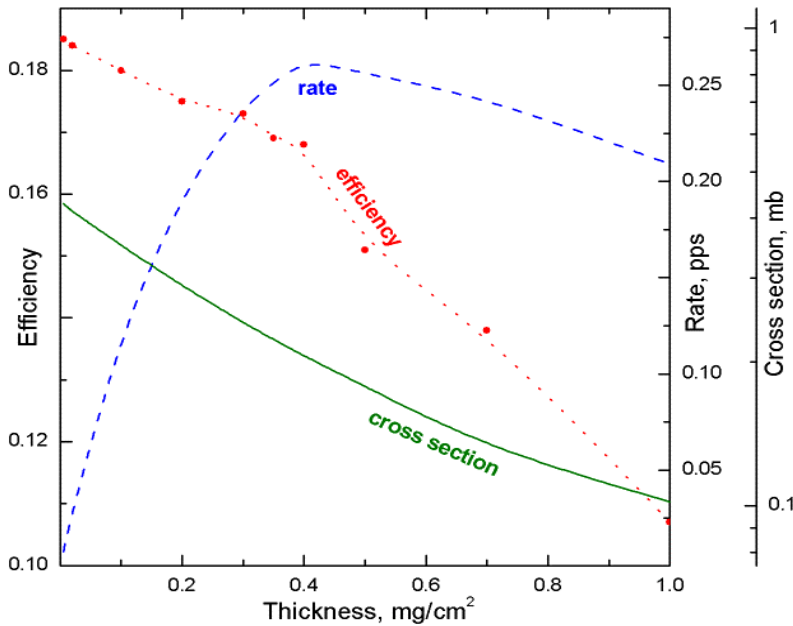
Fig.28. Separation efficiency, production cross section of ^{215}Ac, and rate of all charge states of the residue ^{215}Ac as function of the target thickness calculated by LISE++ for the VAS-SILISSA separator in the reaction ^{22}Ne(100MeV) + ^{197}Au. Cross sections are calculated considering the energy of the primary beam in the middle of the target using the LisFus model ($\hbar\omega = 3$ MeV). The efficiency is the ratio of all charge states of ^{215}Ac at the final focal plane of VASSILISSA separator relative to the number of ^{215}Ac nuclei produced in the target. The separator was always tuned to the ion ^{215}Ac^{8+}.

4.3. Gas-filled magnetic dipole

The gas-filled magnetic block is a more complicated optical block in the code and consists of two classes: magnetic dipole and compound materials. The gas-filled dipole window in the "Set-up" window is shown in Fig.29, where **Br** is the magnetic rigidity [T m], the middle

Fig.29. Gas-filled dipole window in the "Set-up".

string classifies the gas in the dipole and its pressure [Torr], and the bottom line shows a charge state value to which the dipole set, or a mean charge state of the setting fragment after the dipole, if this option was set. The gas-filled dipole dialog is shown in Fig.30.
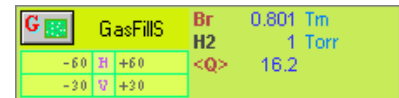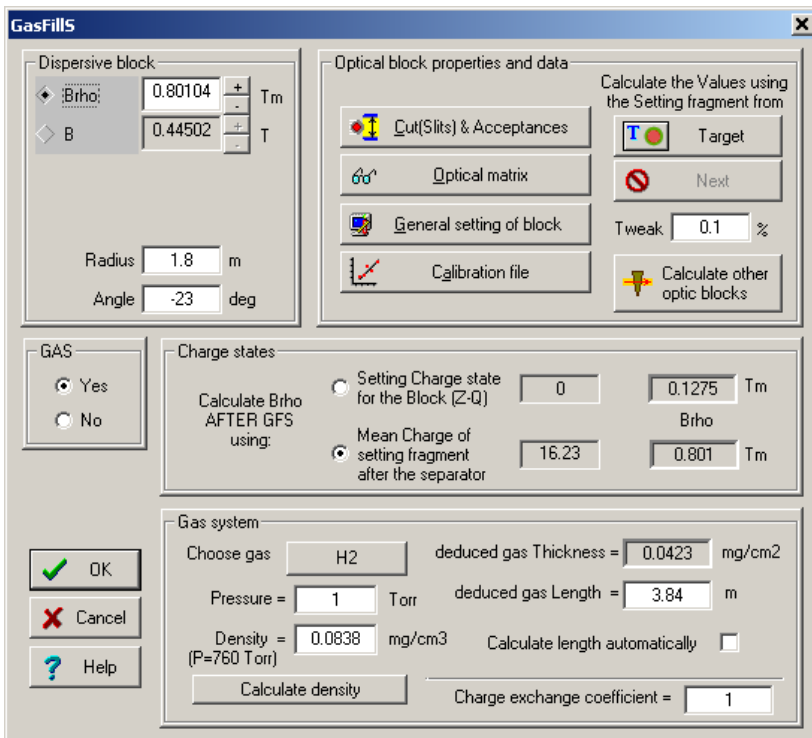
Fig.30. The gas-filled dipole dialog.

The gas-filled dipole is acting as a regular magnetic dipole if the option "GAS" was set to "No" (see Fig.30). In that case the user can see the message "no gas" in the middle string of the gas-filled dipole window in the "Set-up" window (see Fig.29). In the case of no gas different charge states of an isotope end up in different spots after a dipole compared to a magnetic dipole. But if the option "Gas" is set to "Yes" and even the pressure is equal to 0 Torr, the code is suggesting equilibrium of charge states within the gas, and all charge states of one isotope have the same spatial distributions.

It is recommended:

- To use the gas-filled dipole option "Charge states" to set "Mean charge". The option "charge state Z-Q" is applied for debugging purposes or in the case of no gas in the dipole. If the option "Charge States" in the code is set to "Off" (dialog "Preferences") then the field "charge state Z-Q" in the gas-filled dipole is disabled. The code automatically recalculates magnetic rigidity values corresponding to different charge state options and shows them in the dialog. If you want to set one of these values to the dipole setting it is necessary to click the button of the previous block (for example in Fig.30 this button is called "Target");

- To turn off the charge state option in the code if you use just a gas-filled dipole without any other optical dispersive blocks. This avoids time-consuming calculations. If you use other blocks (a magnetic dipole or Wien velocity filter for example) then turn on the charge state option.

It is possible to enter the gas density (for pressure equal 760 Torr) manually or to calculate it (button "Calculate density") by using the new subroutine of the gas density calculation (see the chapter "5.1. Gas density calculations in the dialog "Material"").

It is known that the $B\rho$-resolution is mainly determined by statistics of charge-exchanging collisions, multiple scattering, velocity dispersion and beam optics. The code takes into account energy loss, angular and energy straggling of the fragments in the gas assuming the gas as regular material with reduced thickness calculated using the length of the block and the density of gas. The contribution of charge-changing collisions is given by M.Paul et al.[Pau89]:

$$\Delta x = k_{exch} \cdot Disp \cdot \frac{\Delta q}{\overline{q}} \cdot \frac{100\%}{\sqrt{N_{t\,arg}}\sigma}\ [mm], \qquad\qquad /3/$$

where N_{targ} is the number of atoms in gas [1/cm^2], $Disp$ is the dispersion [mm/%], $\overline{q}$ is the mean charge of ion after the gas, Δq is the standard deviation of a mean value of the charge distribution, k_{exch} is the coefficient used in LISE++ with a default value equal to 1 (see "Charge Exchange Coefficient" Fig.30), and σ is the charge-changing cross section [cm^2] which is calculated by using the empirical scaling rule developed by A.Schlachter et al.[Sch83].

4.3.1. Gas pressure optimization plot

The choice of the gas pressure in a gas-filled separator plays a crucial role for the spatial resolution in the final focal plane of separator. The utility to optimize the gas pressure has been developed in the framework of the LISE++ code. Use the menu "Utilities → Gas pressure optimization for gas-filled dipole" to start the gas pressure optimization (see Fig.31). Different characteristic calculation results versus gas pressure are shown in Fig.32. LISE++ calculated widths in the focal plane of the gas-filled separator as a function of the gas pressure (nitrogen) for ^{41}K, ^{58}Ni, and ^{126}Te ions at the specified incident energies are given Fig.33.
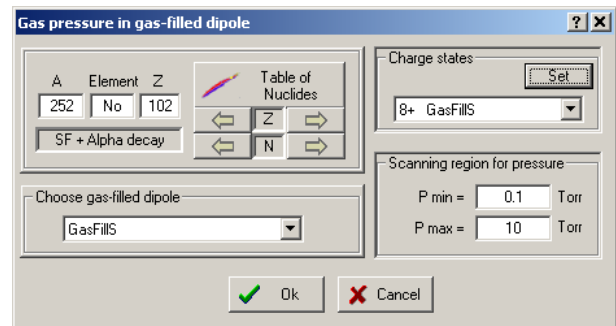

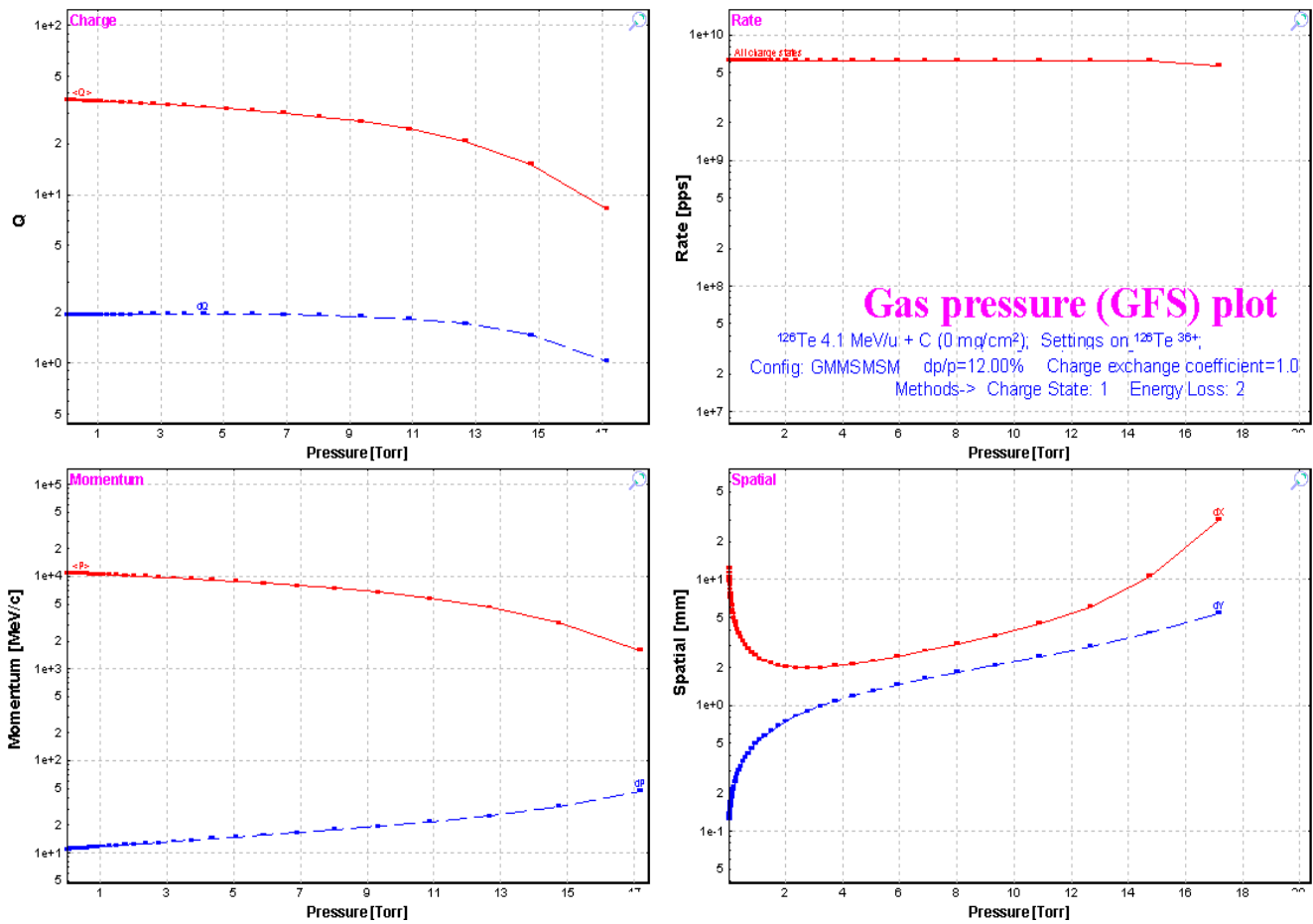**Fig.31.** *The dialog to initialize gas pressure optimization calculations.*
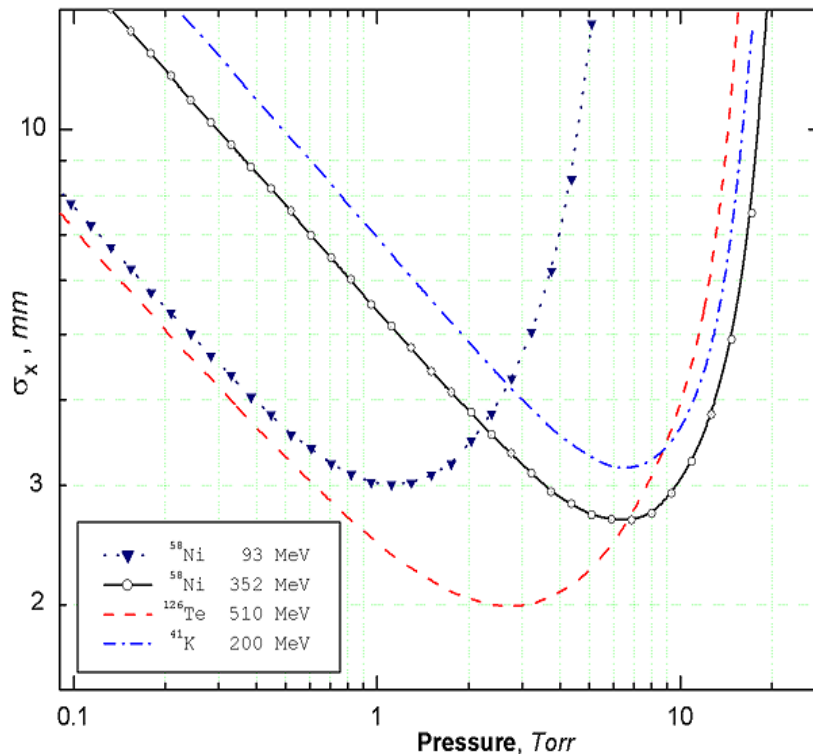
Fig.32. The gas pressure optimization plot.

Fig.33. LISE++ calculated widths in the focal plane of the gas-filled separator as a function of the gas pressure (nitrogen) for ^{41}K, ^{58}Ni, and ^{126}Te ions at the specified incident energies. The incident ions were chosen to compare to the paper [Pau89]. To calculate this plot the incident ions were assumed as primary beam. The dipole length was set to 3 meters, and the target thickness equal zero was used. The optical matrix of the separator is unitary except for the dispersion which is equal to 10 mm/%. The primary beam emittance was set to x=y=±0.1mm, x'=y'=±0.1mrad, dP/P=±0.1%. The example discussed in the figure can be found on the LISE web-site: http://www.nscl.msu.edu/lise/6_2/examples/paper_gfs.lpp

4.3.2. The Dubna GFS configuration

The LISE++ configuration file (Lise/config/Dubna/Dubna_GFS.lcn) of the Dubna gas-filled separator has been created parameters given an using the articles [Oga98] and [Sub02]. However it is still necessary to correct the

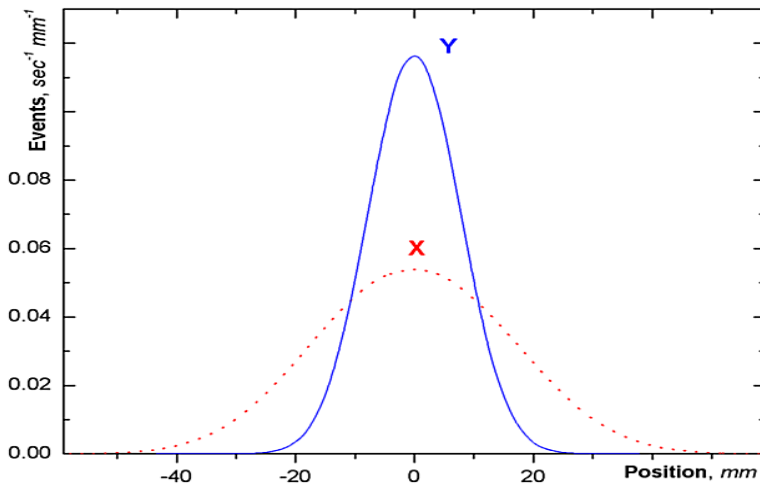**Fig.34.** *Dubna gas-filled separator scheme*

optical matrix of the dipole. The scheme of the spectrometer is shown in Fig.34. Spatial distributions of ^{252}No residues at the focal plane of the separator are given in Fig.35. This example of the transmission residues in the Dubna gas-filled separator from the reaction ^{48}Ca(217MeV) + ^{206}Pb(0.4 mg/cm^2) $\rightarrow$ ^{252}Ac can be found in the file "Lise/Files/Dubna_GFS.lpp" which is

Fig.35. *Horizontal and vertical focal-plane position spectra in the reaction ^{48}Ca(217MeV)+^{206}Pb $\rightarrow$ ^{252}No+2n calculated by LISE++.*

included in LISE++ package.

5. New features and Corrections

5.1. Gas density calculations in the dialog "Material"

LISE++ has a database containing various densities for materials in a solid state. In case of gases it is difficult to create a similar database of densities because the gas density depends on pressure and temperature. In this context the gas density dialog was created (see Fig.36), in which the user can enter parameters of the environment (gas and pressure) to calculate the density of a gas. The dialog is loaded from the material dialog in the mode "Gas" (Fig.37). Also in the mode "Gas" the user can enter parameters of a molecular gas. The units converter can be called from the gas density dialog to transform units of temperature or pressure.
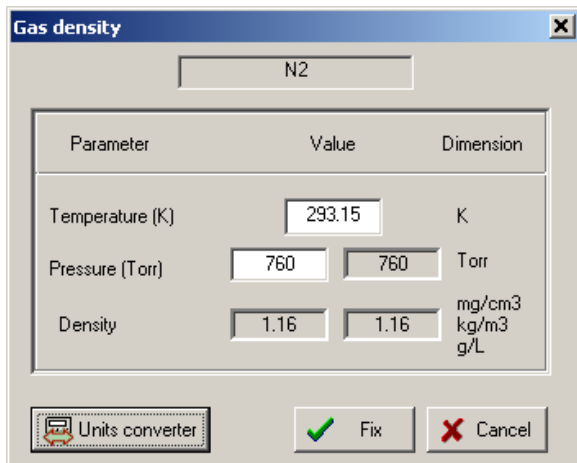
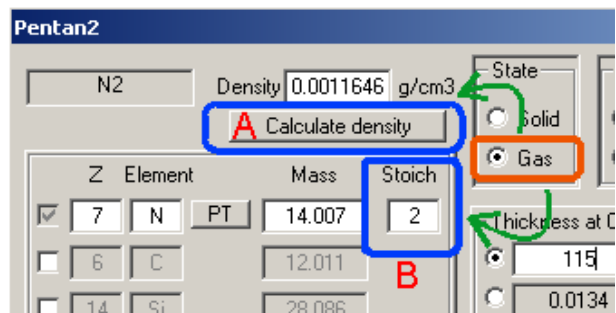**Fig.36.** *Gas denity dialog.*

Fig.37. *The segment of the material dialog in the mode "Gas". The button "Calculate density" (letter "A") and the field "Stoich." (letter "B") to enter a molecular gas appear in the mode "Gas" of the material dialog.*

5.2. The "Beam" dialog: several possibilities to enter a beam energy

The opportunity was created to set the energy of the primary beam in the "Beam" dialog (see Fig.38) through various equivalent physical quantities. So for example in the region of intermediate energies it is convenient to enter the energy in MeV per nucleon, while for low energies it is common to quote the total kinetic energy of the projectile.
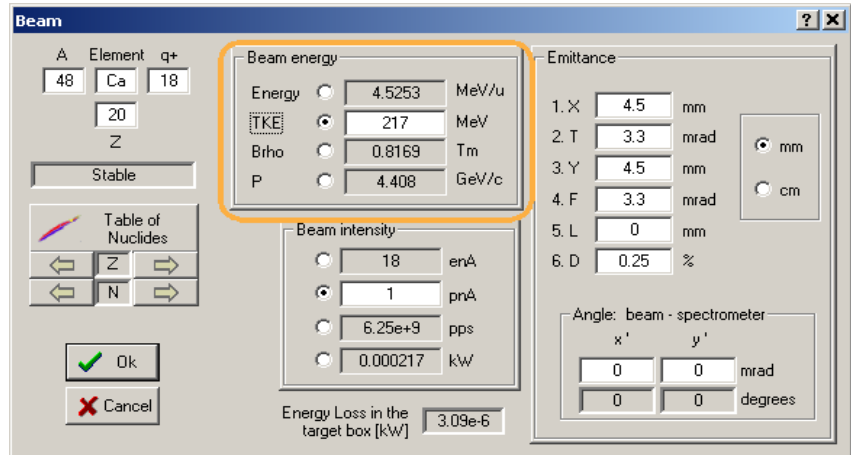

Fig.38. The Beam dialog.

5.3. Spectrometer setting for the primary beam in the fusion mode

In case of fusion-evaporation reactions the program considers the entered primary beam particle as product of the reaction. If the user sets a nucleus as fragment (residue) in the regular way, then the program will apply the cross section, and angular as well as momentum distributions calculations assuming a fusion-evaporation reaction. However it is often desired to see the trajectory and the transmission of the primary beam particles. For this purpose it is

Fig.39. The fragment of the Set-up window in the case when the primary beam is set as setting fragment.

possible to set the primary beam as fragment in the menu "Settings → Tune the spectrometer for primary beam". The message "=beam=" will appear close to fragment settings in the Set-up window (see Fig.39). The program automatically calculates the spectrometer settings optimal for the primary beam transmission. Charge states of the primary beam for the spectrometer can be entered using the optical block dialogs.
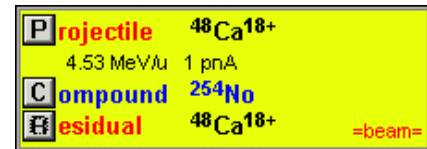
5.4. Angular straggling

A new method [PDG00] to calculate angular straggling has been added to the program. The opportunity to perform calculations without contributions of angular and energy straggling (for debugging purposes) are included in the program (see the dialog "reaction mechanism"). The user now can compare different models for angular straggling versus projectile energy using the menu "Utilities → Plot of angular straggling in the material".

For calculations of angular straggling at small energies arises the question at what energy the formula remains valid? So in the work [Dio89] it was assumed that using the model is correct only if the scattering angle is below 10 degrees. The use of the Born approximation is expected to be valid when the born parameter α_B is much smaller then unity. In the nonrelativistic approximation this condition is satisfied if

$$\alpha_B \sim \frac{Z_1 \cdot Z_2}{137\beta} \quad << \quad 1. \qquad\qquad /4/$$

However, R. Anne et al [Ann88] have shown that experimental results obtained in the reaction ^{100}Mo(23.8MeV/u)+Au (α_B=109.2) are in the good agreement with the calculations. To avoid problems with calculations at energies close to zero (when the angular straggling value begins to become infinite) the following restriction for the energy is applied:

$$E_{limit} = \frac{Z_t \cdot Z_p}{2 \cdot A_p \cdot A_t^{0.55}} [MeV/u],$$ /5/

where Z_t, Z_p are the atomic number for the target and projectile and A_t, A_p are their mass numbers respectively. The coefficient has been chosen so that the lateral range is always monotonically increasing for increasing energy and every combination of projectile and target. The plot of the fragment range in material (see menu "Utilities") was used for this purpose. Angular straggling models use E_{limit} for calculations for projectile energies below E_{limit}.

5.5. Corrections and changes

Some updates and corrections have been included in version 6.2 compared to the previous version. Items affected by the changes are listed below:

- Monte Carlo 2D plot,
- Wedge dialog,
- Momentum distribution after the stripper,
- Rotation block transmission,
- The Optic Block Dialog,
- Total Kinetic energy plot (1D) from the menu
  "Plot → Total kinetic energy distributions" (see Fig.40),
- LISE++ file (*.lpp) for option "charge state is ON",
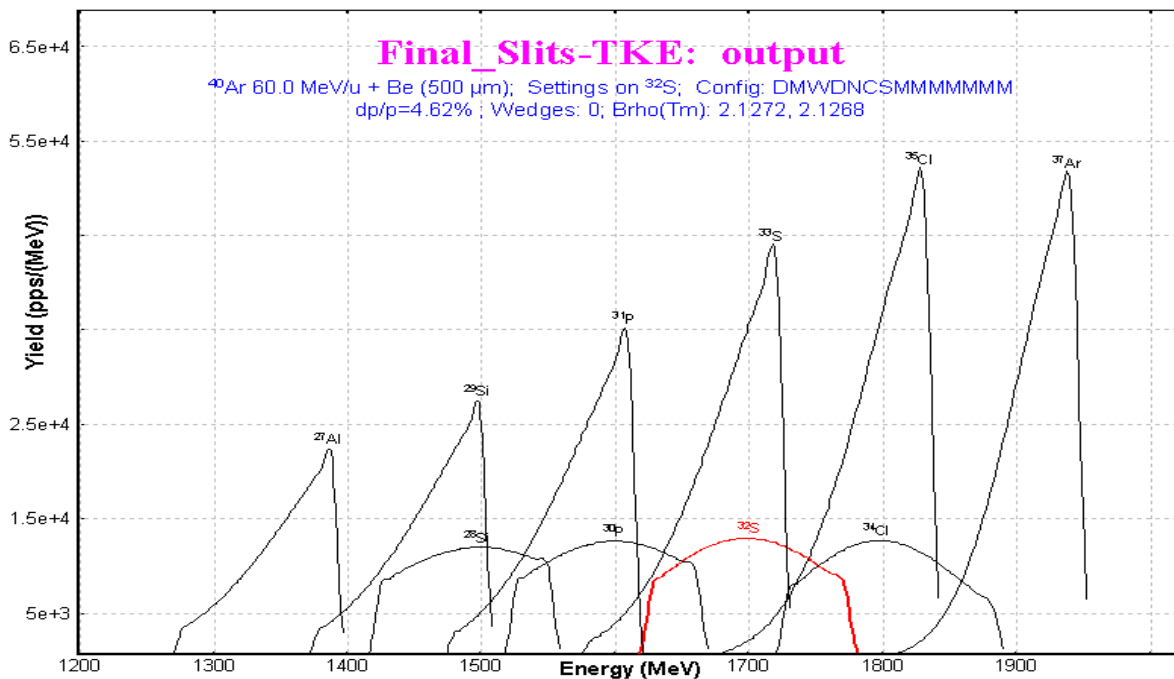- Angular transmission calculations.

Fig.40. Total kinetic energy distribution plot.

6. Sub-barrier fusion cross-section

The possibility to calculate sub-barrier fusion cross section is available now in the PACE4 code as well as in the LisFus model. There is a brief introduction for the quantum-mechanical approach used in the codes. The cross section for the compound-nucleus formation is given as

$$\sigma = \pi \hat{\lambda}^2 \sum_{l=0}^{\infty} (2l+1) T_l , \qquad\qquad /6/$$

where T_l is the transmission coefficient for the lth partial wave:

$$T_l = \left\{ 1 + \exp\left[\frac{l - l_{max}}{\Delta} \right] \right\}^{-1} , \qquad\qquad /7/$$

with Δ as diffuseness parameter and l_{max} as the maximum angular momentum determined by the total fusion cross section. This approach was used in the code PACE [Gav80]. For the study of fusion reactions below the Coulomb barrier it is necessary to use the quantum-mechanical transmission probability instead of the classical solution to describe the experimental data. For a one-dimensional barrier it is assumed that the potential barrier can be replaced by a parabola:

$$V_0(r) = V_{B0} - \tfrac{1}{2}\mu^2 \omega^2 (r - r_0)^2 , \qquad /8/$$

where V_{B0} is the barrier height and ω is a measure of the curvature of the s-wave potential barrier. The transmission probability can be calculated following [Hil53]

$$T_0(E) = \left\{ 1 + \exp\left[\frac{2\pi(V_{B0} - E)}{\hbar\omega} \right] \right\}^{-1} . \qquad /9/$$

Fig.41. *Classical (on the left) and quantum-mechanical (on the right) transmission probabilities for a one-dimensional potential barrier [Bal98].*

In a completely classical treatment, T_0 is unity above the barrier and zero below, as shown in Fig.41. Quantum mechanically the $dT_0(E)/dE$ delta function peak is broadened [Bal98] as the transmission probability smoothly evolves from zero at energies far below the barrier to unity for energies far above the barrier (see Fig.41).

It is possible to approximate the l dependence of the transmission probability at a given energy by simply shifting the energy [Bal98]:

$$T_l \cong T_0 \left\{ E - \frac{l(l+1)\hbar^2}{2\mu R^2(E)} \right\} , \qquad\qquad /10/$$

where $\mu R^2(E)$ characterizes an effective moment of inertia. Approximating $R(E)$ by r_0 and inserting the penetration probability for the parabolic barrier, one obtains an approximate expression for the cross section [Won73]:
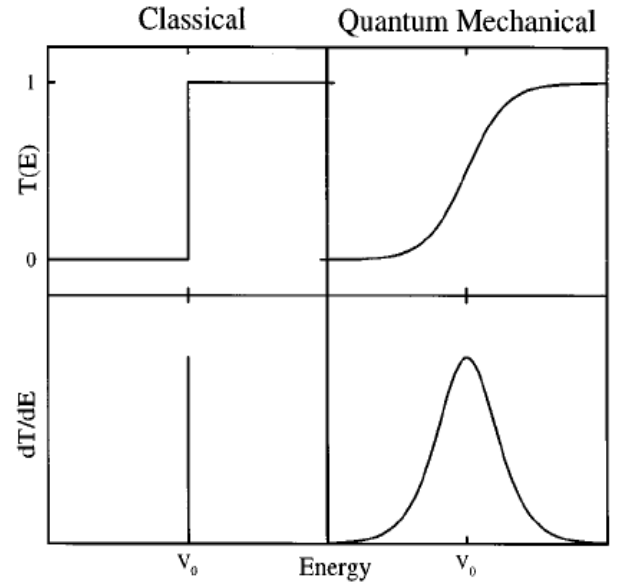
$$\sigma(E) = \frac{\hbar \omega r_0^2}{2E} \log \left\{ 1 + \exp \left[\frac{2\pi (E - V_{B0})}{\hbar \omega} \right] \right\}. \qquad /11/$$

In the classical limit, where $\omega \to 0$ or $E \gg V_{B0}$, Equation /11/ reduces to the standard geometrical result:

$$\sigma(E) = \pi r_0^2 \left(1 - \frac{V_{B0}}{E} \right). \qquad /12/$$

The user can choose the calculation method of the transmission probability for a potential barrier in the "Fusion-evaporation settings" dialog (see Fig.42) in LISE++. The default value of the curvature parameter is equal to 5 MeV. The same option exists in the PACE4 code in the "Card 2-1" dialog. Cross section calculations by the PACE4 program and the LisFus model for the example

Fig.42. The dialog of fusion-evaporation settings

reaction ^{197}Au(^{22}Ne, 3-6n) using the quantum-mechanical transmission probability for the potential barrier are given in Fig.43 and Fig.44. This reaction was already used for residue transmission calculations in chapter "4.2.6. Residue transmission calculation" compared to experimental results from the paper [Yer94].
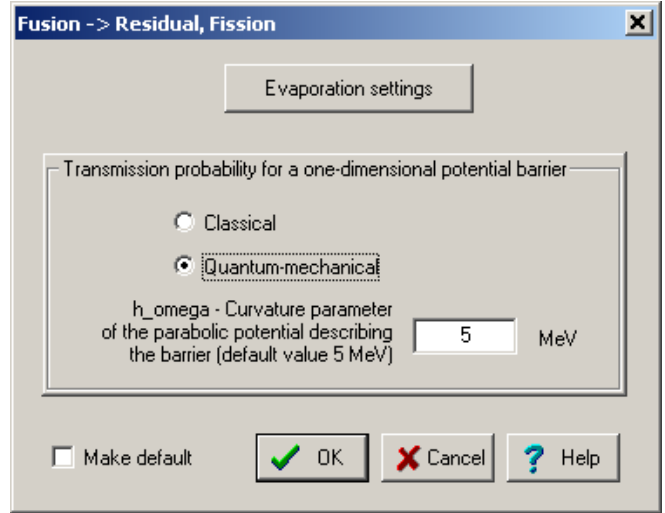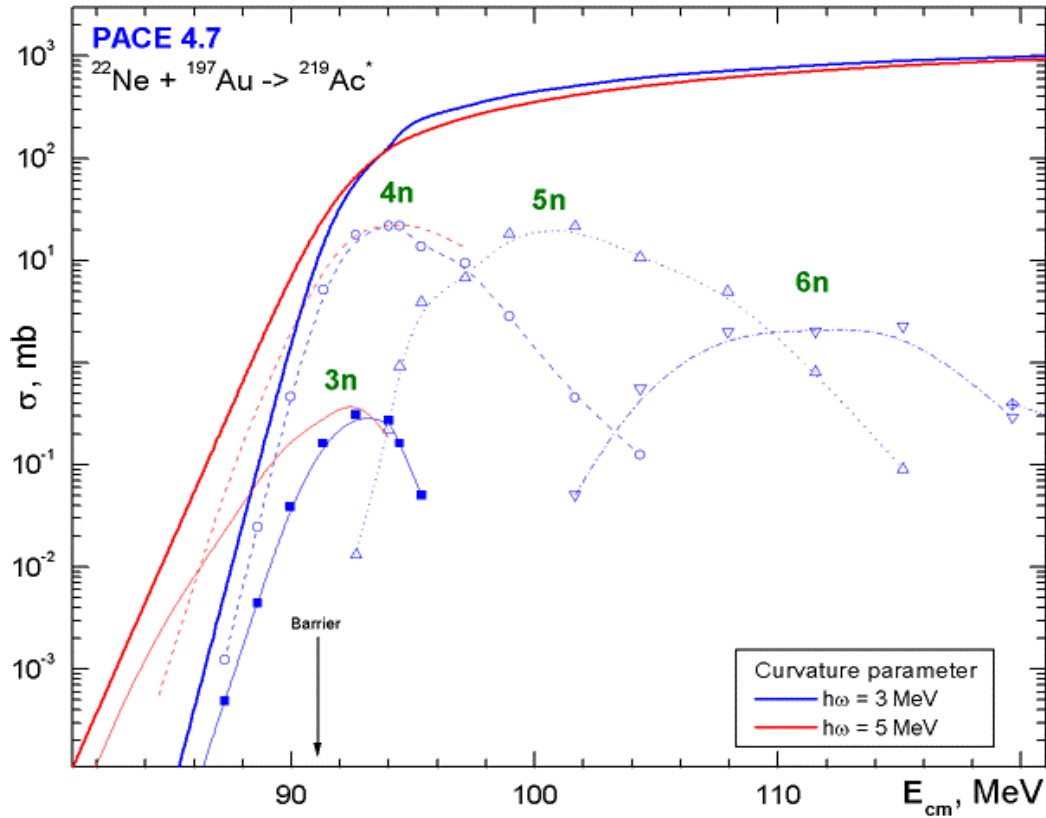
Fig.43. *PACE calculated fusion-evaporation cross sections for the reaction $^{197}Au(^{22}Ne,3\text{-}6n)$ using the quantum-mechanical transmission probability for the potential barrier using the two different values of the curvature parameter 3 and 5 MeV.*
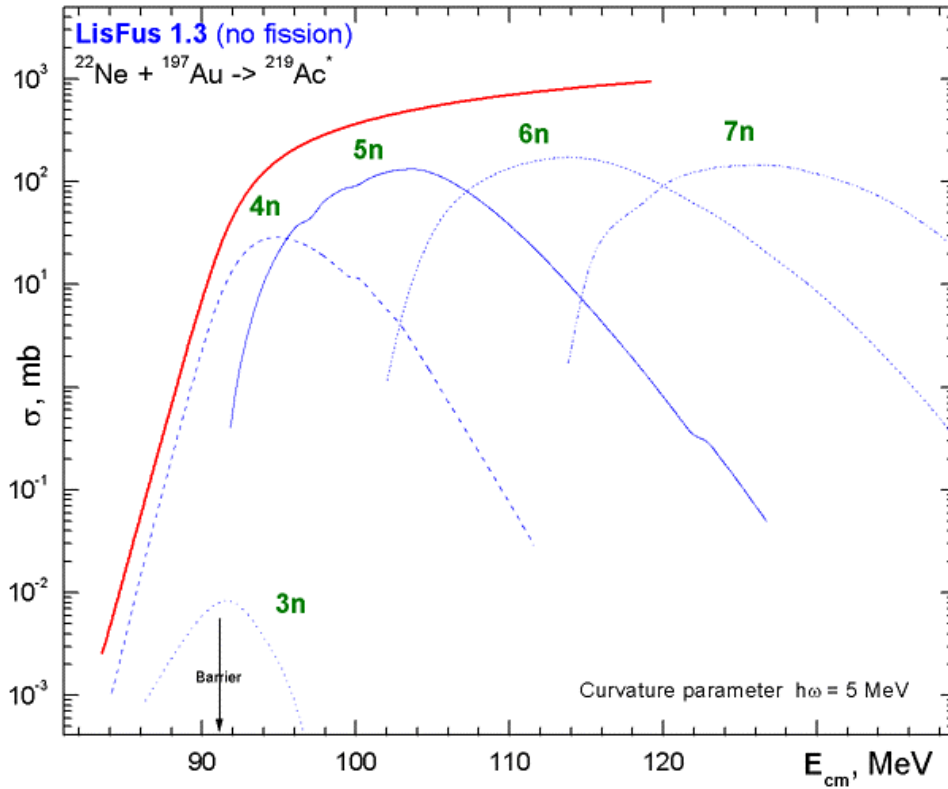

Fig.44. *LisFus calculated fusion-evaporation cross sections for the reaction $^{197}Au(^{22}Ne,3\text{-}7n)$ using the quantum-mechanical transmission probability for the potential barrier with the curvature parameter equal to 5 MeV.*

7. The code "BI" development

The program "BI" for the automatic search of two-dimensional peaks has undergone a number of changes: cycles optimization, some corrections, and help support has been included.

Contour and projection utilities allowing to work with experimental spectra have also been added. The user can create a contour using the icon in the toolbar of the plot window
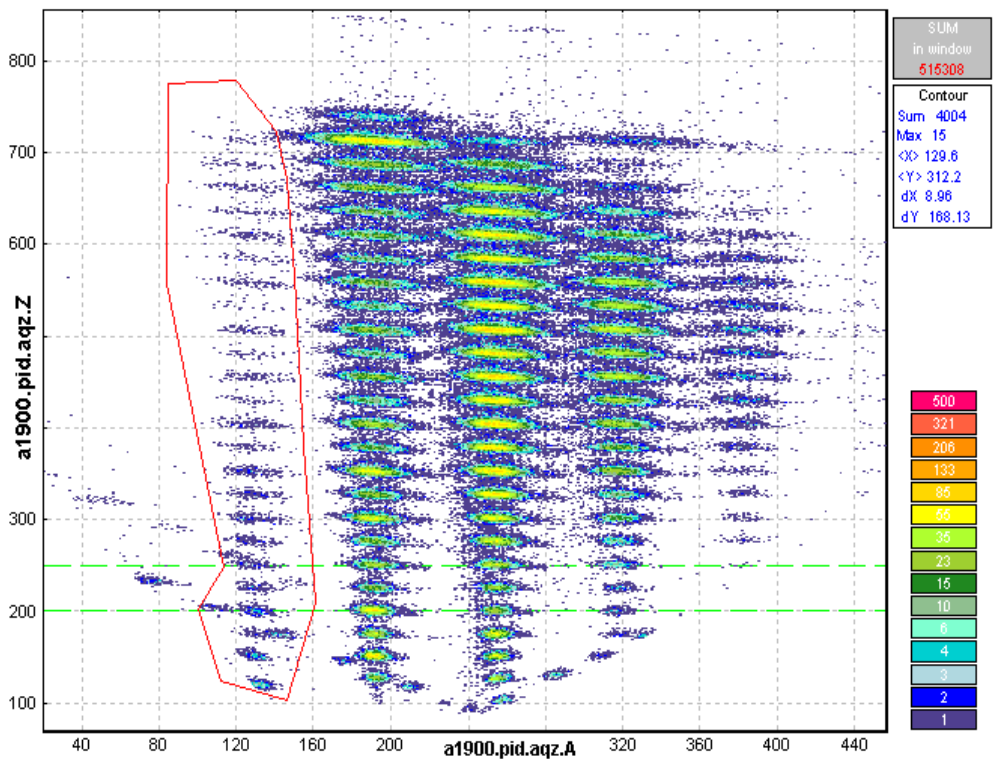

Fig.45. *Example of a contour in a two-dimensional particle identification plot. Statistic characteristics of the data within the contour are shown in the top right window.*
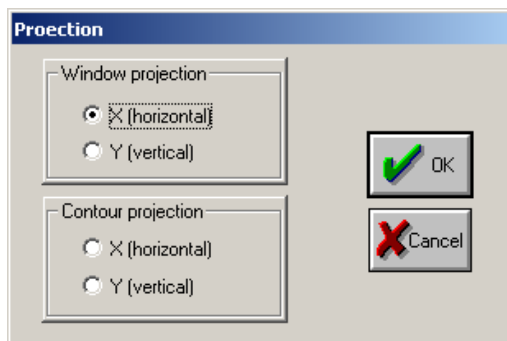
while displaying an experimental two-dimensional spectrum. By pressing the left mouse button, the user can add a new point of a contour, while pressing the right mouse key closes the contour. Statistic characteristics of the data within the contour will appear in the top right window of the plot (see Fig.45). The contour can be used in the case of low intensity two-dimensional peaks or bad separation between them. Under these conditions the program cannot identify peaks automatically. The user can manually get the peak characteristics or create a contour projection on one of axes.

By pressing the icon ![P] the user loads the projection dialog (see Fig.46) which prompts to choose a method to create a projected spectrum. The projection of the contour in Fig.45 on the vertical axis is shown in Fig.47. The one-dimensional spectrum can be saved as a file using the icon ![save] for a further analysis by the code "Bi" in the one-dimensional peak search mode.
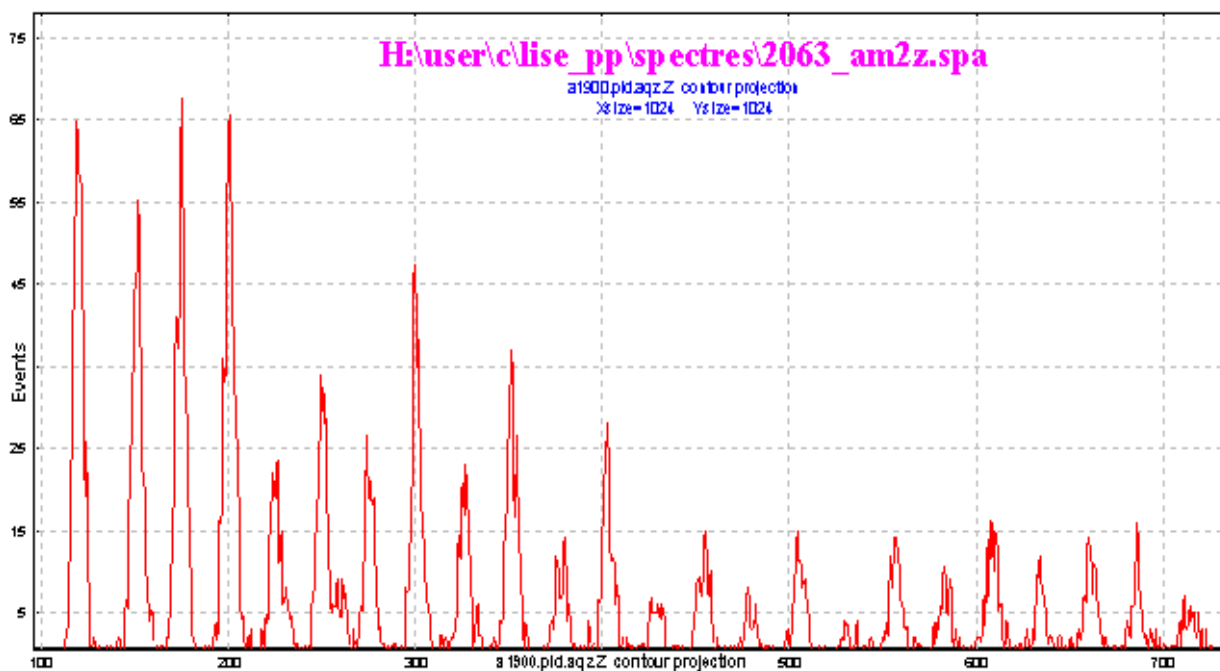

Fig.47. One-dimensional spectrum obtained from the contour projection (see Fig.45) onto the vertical axis.

8. Future perspectives for LISE++ (version 6.3)

- Incorporate the "Global" code in the LISE++ package.

- Add the fission channel in the LisFus model.

- Develop fission products kinematics in LISE++.

- Incorporate a new reaction mechanism: **Fission**.

Acknowledgements

References:

[Ann88] R.Anne et al., NIM B34(1989) 295-308.

[Bal98] A.B.Balantekin and N.Takigawa, Rev.Mod.Phys. 70 (1998) 77-99.

[Dio89] J.S.Dionisio et al., NIM A282 (1989) 10-21.

[Hil53] D.L.Hill and J.A.Wheeler, Phys.Rev.89 (1953) 1102.

[Oga98] Yu.Ts.Oganessian, et al. Proceedings of Fourth International Conference on Dynamical Aspects of Nuclear Fission, 19–23 October 1998, Casta-Papiernicka, Slovak Republic, World Scientic, Singapore, 2000, p. 334;

[Pau89] M.Paul et al., NIM A277 (1989) 418-430.

[PDG00] Particle physics booklet; http://pdg.lbl.gov

[Sch83] A.S.Schlachter et al., PRA 27 (1983) 3372-3374.

[Sch98] C.Scheidenberger, Th.Stohlker, W.E.Meyerhof, H.Geissel, P.H.Mokler, B. Blank, NIM B 142 (1998) 441-462; http://www-aix.gsi.de/~scheid/CHARGE.html

[Sub02] K.Subotic et al., NIM A 481 (2002) 71–80.

[Thi85] P.Thieberger, H.E.Wegner, J.Alonso, H.Gould, C.Munger, R.Anholt, W.E.Meyerhof, IEEE Trans. Nucl.Sci. 32 (1985) 1767.

[Tri89] R.E.Tribble, R.H.Burch, C.A.Gagliardi, NIM A 285 (1989) 441-446.

[Won73] C.Y.Wong, Phys.Rev.Lett. 31 (1973) 766.

[Yer94] A.V.Yeremin et al., NIM A350 (1994) 608-617.